Safety Analyses for the UMass-Lowell Research Reactor (UMLRR)

Dr. John R. White

Chemical and Nuclear Engineering Department
University of Massachusetts Lowell
Lowell, MA 01854

August 17, 2015

I. Introduction/Overview

A series of studies are currently on-going to support the re-licensing of the UMass-Lowell research reactor (UMLRR). A key element of the required Safety Analysis Report (SAR) for the license submittal is the accident analyses that eventually will be formally described in Chapter 13 of the SAR. NUREG-1537 (see Ref. 1) gives a good overview of the type of accidents that should be considered, including both anticipated events such as the loss of normal electrical power or a malfunction of an experimental device, and hypothetical events such as the maximum hypothetical accident (MHA) that postulates the failure of a fuel plate (with no detail about what causes the failure) and subsequent release of a portion of its fission product inventory to the reactor pool. This report, however, only addresses the credible accident scenarios that eventually lead to either a reactivity-induced transient or a flow-induced transient within the reactor. For example, it is certainly feasible that a near step change in reactivity or a ramped reactivity insertion could result from a sudden failure of an experiment or from a control blade drive malfunction, respectively, and the consequences of such reactivity events must be understood and restricted to be below established safety guidelines. Likewise, a loss of flow scenario would occur with a pump failure or a loss of electrical power event, so the sequence of events following a loss of flow accident must be evaluated to guarantee that no safety limits are exceeded.

The safety analyses performed here are strongly reactor-specific, so lots of pertinent information about the physical system and several UMLRR-specific operational characteristics are also discussed and summarized for future reference. For example, the physical characteristics of the fuel assembly, fuel plate, and coolant channel geometry are clearly important for any safety studies -- with data and analyses documented for both the UMLRR U_3Si_2-Al and WPI UAl_x-Al fuel types so that, after NRC approval, both fuel types can be used as needed within the UMLRR. Additionally, knowledge about the axial and radial flux and power profiles (i.e. peaking factors), the blade worth distributions, and the coolant flow distribution within the fuel elements and the various bypass channels is required, along with a set of kinetics parameters, reactivity coefficients, etc.. Thus, a lot of preliminary information is included in this document to provide a full set of reference specifications and conditions for the overall UMLRR safety analyses performed here.

The remainder of this report summarizes the computational models, input data, analysis assumptions, and overall results of the safety analyses performed for the UMLRR. It is expected that much of the information presented here will serve as the basis for appropriate portions of the SAR to be submitted as part of the UMLRR license renewal -- so lots of material is included to provide full detail of the analyses completed as part of this effort.

II. Reactor Overview, Fuel Element Designs, Control Considerations, Etc.

The UMass-Lowell research reactor (UMLRR) is a water moderated and cooled open pool-type reactor that has a flat-plate fuel element design. The fuelled core region is reflected primarily by a combination of water basket and graphite reflector elements. The standard UMLRR low enriched uranium (LEU) fuel design uses uranium-silicide U_3Si_2-Al fuel, with 200 g of U235 per element. The UMLRR also currently has a possession-only license for 27 slightly used uranium-aluminide UAl_x-Al LEU fuel elements that were obtained from the Worcester Polytechnic Institute (WPI) when their research reactor was shut down.[2] The UMLRR U_3Si_2-Al and WPI UAl_x-Al fuel elements are similar in overall size and shape, so both elements fit interchangeably within the UMLRR grid support structure. However, the material composition of the fuel meat is different (aluminide vs. silicide fuel), the U235 loading is quite different (167 g for the WPI element vs. 200 g for the UMLRR assembly), the number of fuel plates per element differs (18 vs. 16 for the WPI and UMLRR fuel, respectively), and there are also some small differences in meat thickness, plate thickness, water gap thickness, etc., so formal analyses that include both types of fuel design are required. A detailed comparison of the two fuel types is given in Table 1 -- and the data given here were used in all the physics and thermal hydraulics models developed as part of this work (also see Ref. 3 for a more detailed comparison of the two fuel element types and Ref. 4 for an analysis of the behavior/performance of the WPI elements within the WPI reactor). As detailed later in the current report, the UMLRR physics and safety analysis studies were performed for a variety of core arrangements containing only UMLRR fuel, only WPI fuel, and for a variety of mixed core configurations. In all cases, the original UMLRR uranium silicide fuel is shown to be more limiting than the WPI fuel element, primarily because it is more reactive due to its higher U235 loading and it has a higher average plate power due the smaller number of fuel plates per element. By studying both fuel types in a variety of configurations, we have established that any reasonable homogeneous or mixed core configuration (that meets the UMLRR Technical Specifications criteria for excess reactivity and shutdown margin) should be acceptable for use within the UMLRR.

The core grid plate, consisting of a 9 by 7 rectangular array of spaces in an egg-crate shaped bottom aluminum plate, is capable of being loaded with fuel elements, reflector elements (graphite or water), experimental radiation baskets, and lead-void boxes. The availability of both water and graphite reflector elements gives flexibility in adjusting the core excess reactivity by simply interchanging some of the water vs. graphite elements closest to the fuel. The Pb-void elements were installed within the UMLRR in 2002 as part of a new core arrangement (the M-2-5 core) that included a new experimental facility, referred to as the fast neutron irradiator (FNI), on one side of the core. For proper operation of the FNI, neutron moderation needs to be minimized, so the use of water and/or graphite elements between the last fuel row and the FNI is totally inappropriate. Instead, the Pb-void elements provide about 1″ of primary gamma shielding and they also tend to neutronically de-couple the core region from the remainder of the FNI facility. More importantly from the FNI perspective, however, is that these elements do not significantly decrease the fast flux (see Refs. 5 and 6 for more details of the FNI design and associated core configuration changes).

In addition to the FNI, the UMLRR also has a number of additional experimental facilities, including three beam tubes, a graphite thermal column, a pneumatic tube assembly, and several in-core radiation basket elements. Two radiation basket types, water-filled and graphite-filled, are available, where the two designs are nearly identical except for the material contained in the

region between the inner Al tube (where an experimental bayonet can be inserted) and the outer Al can. In particular, a single graphite radiation basket was designed specifically to be placed in the center of the core (D5 location) to create a centrally located flux trap region with high thermal flux, with the graphite basket design being selected for this location simply to minimize power peaking in the nearby fuel assemblies -- since graphite gives a lower peak thermal flux in the neighboring fuel locations relative to water.

Table 1 Physical data for the UMLRR and WPI standard fuel elements.

Parameter	UMLRR Full Fuel Element	WPI Fuel Element
Plate Data:		
fuel type	U_3Si_2-Al	UAl_x-Al
enrichment (w/o)	19.75	19.75
U235 loading (g/plate)	12.5	9.28
plate width (cm)	7.140	7.049
meat width (cm)	6.085	6.085
plate thickness (cm)	0.1270	0.1524
meat thickness (cm)	0.0510	0.0762
clad thickness (cm)	0.0380	0.0381
plate height (cm)	63.50	62.55
meat height (cm)	59.69	59.69
Assembly Data:		
fuel plates/element	16	18
aluminum plates/element	2	0
U235 loading (g/element)	200.0	167.0
side plate thickness (cm)	0.5080	0.4572
channel thickness (cm)	0.2963	0.2709
assembly dimension (cm × cm)	7.620 × 7.620	7.620 × 7.620
assy. dim. with gap (cm × cm)	7.7724 × 7.7724	7.7724 × 7.7724

Concerning the D5 flux trap experimental location, it should be noted that during some scheduled maintenance in May 2015 it was discovered that the graphite basket element had swollen beyond tolerance, and could not be replaced back into the core. As discussed in Ref. 7, an interim solution that met immediate reactivity and peaking factor requirements was to replace the damaged graphite basket element with a graphite reflector. However, this choice is certainly not ideal, since it eliminates an important experimental facility within the UMLRR. Thus, the current M-2-7 core (i.e. the M-2-5 arrangement with a graphite reflector in D5) is only a temporary configuration until a more suitable replacement for the damaged graphite basket

element can be obtained (see further discussion on this subject in the next section, "The Reference Core Design").

Reactivity control in the UMLRR is accomplished with four large safety blades and one low-worth regulating blade (i.e. the RegBlade, for short). The neutron poison material in all the control elements is B_4C in various geometries and loadings. The RegBlade, for example, looks like a hollow square, with three sides of the square geometry made from Boral plates containing a 35 w/o B_4C composition, with the last side consisting of an aluminum plate of the same thickness as the Boral plates.[8] This arrangement allows some flexibility in establishing the total RegBlade worth, since the element can be rotated to have the poison material facing towards or away from the fuel region, allowing either a "high worth" or "low worth" arrangement, respectively. The "high worth" configuration has been in use since the HEU to LEU fuel conversion took place back in Aug. 2000.[9-10]

Concerning the large safety blades, there is a project currently underway to physically replace the original blades because of some blistering that has been observed with one of the existing blades (in particular, Blade 3). In planning for the blade replacement, a discrepancy was discovered with the blade description given in the original UMLRR FSAR.[8] In particular, the original GE blade blueprints suggest that the Boral poison material already has an inherent Al clad, and that this composite material is then inserted in an aluminum clad to make up the control blade for the UMLRR -- essentially giving the 50 w/o B_4C Boral poison a double layer of Al clad (the poison layer in this model is only 0.125 inches thick). In contrast, the drawing in the original FSAR suggests that the Boral poison layer is 0.255 inches thick and only contains a single clad layer of about 0.06 inches. In addition, since the FSAR did not explicitly describe the B_4C-Al mix in the Boral, a 35 w/o B_4C composition was assumed, which is the stated composition of the regulating blade.[8] This contradictory information about the control blades created a brief dilemma, since the current computational models of the UMLRR give reasonable blade worth comparisons to measured data, yet these models are based on the original FSAR diagram.

A single homogeneous metal matrix composite (MMC) material with no explicit clad was selected for the replacement blade design. For the new blades, the neutron poison BORTEC[11] material is a homogeneous MMC mix of B_4C and Al. For the specific UMLRR control blades, a 23 w/o B_4C composition was used with a total thickness of 0.375 inches (which exactly matches the outer dimensions of the original blades).[12]

A preliminary study was conducted to address the dilemma concerning the current blades and to evaluate the relative worth of the new blade design within the UMLRR. The study looked at the total relative worths of the three designs discussed above, as summarized in Table 2. Reference 13 summarizes the numerical results of the study, but the two key conclusions were as follows:

1. The uncertainty in the construction and modeling of the existing blades (FSAR vs. GE DWG models) does not have a significant effect on the predicted blade worth -- there is only a 5-6% difference in the FSAR and GE DWG worth estimates and this is in the range of uncertainty in the experimental measurements.
2. The new MMC blades should have essentially the same worths as predicted by the FSAR model that has been in use for 25+ years (this was expected since the B-10 areal density is essentially the same). Thus, the measured worth of the new blades should be comparable to or slightly greater than the measured worths of the existing blades.

Table 2 Key parameters for three different blade configurations.

Blade Model	Poison Thickness (inches)	B_4C Component (w/o)	B-10 Areal Density (g B-10/cm^2)
FSAR	0.255	35	0.0815
GE DWG	0.125	50	0.0564
MMC	0.375	23	0.0815

Blade 3 was physically replaced with the new MMC control blade in June 2015 within the M-2-7 core configuration (the new arrangement after blade replacement was designated as the M-2-7-A core). A full set of blade worth measurements was made before and after the replacement and the total measured worths are summarized in the last two columns in Table 3. As apparent, the total worth of the new Blade 3 was only slightly higher relative to the original blade (really essentially unchanged since the increase is within experimental uncertainty) -- and the latter portion of this statement is also true for all the other blades as well. The measured results in Table 3 are fully consistent with the conclusions from the computational study reported in Ref. 13. Based on the success of the Blade 3 replacement, the remaining safety blades will also be replaced with the MMC BORTEC material at the next convenient maintenance interval.

Table 3 Measured blade worths (%Δk/k) for three different core configurations.

Blade #	**M-2-5** reference core with graphite basket in D5	**M-2-7** M-2-5 with graphite reflector in D5	**M-2-7-A** M-2-7 with new MMC material for Blade 3
1	2.56	2.69	2.66
2	2.16	2.30	2.25
3	3.29	3.39	3.50
4	3.54	3.59	3.67
total worth	11.55	11.97	12.08

For reference, Table 3 also includes the Jan. 2015 measured total blade worths from the M-2-5 core (which includes the graphite basket in the D5 location). The worth distribution and total worth of Blades 1-4 are very similar to the M-2-7 configuration (which has a graphite reflector in D5). There is, however, a slight consistent increase in the worth of each blade in going from the M-2-5 to the M-2-7 core, which is probably the result of a flattening of the flux profile near the central D5 location, with a corresponding increase in the flux near the control blades. It should be emphasized that the shift is small (only a 3-5% increase), which is still within the expected measurement uncertainty of about 5% -- however, in this case, the slight increase in all the blade worths can be easily rationalized.

The importance of the above discussion to the current study is that many of the safety analysis calculations used data derived from the M-2-5 core with the original FSAR control model. However, although the current and future core configurations certainly will differ somewhat, the

actual M-2-5 core, which was the primary core configuration in use within the UMLRR from early 2002 to May 2015, is expected to be quite representative of any feasible core arrangement that may be considered in the foreseeable future (unless there is a major shift in the purpose of the FNI experimental facility or the incore irradiation zones -- which would then require a completely new core arrangement and a review of how the new configuration fits within the current safety evaluation).

III. The Reference Core Design

As noted above, the M-2-5 core with the original FSAR control blade model was utilized to derive many of the parameters used in the subsequent safety analyses calculations. A sketch of the M-2-5 material configuration is shown in Fig. 1, which clearly identifies the row and column grid notation that has been referred to several times already. For example, the D5 location refers to row D and column 5 in the core grid, which is directly in the center of the core -- this is commonly referred to as the flux trap location. Additionally, one can identify the RegBlade in position D9, a partial fuel element in C3 (which contains half the uranium loading of a full UMLRR fuel assembly), five Pb-void elements in row A, etc.. Also, we should note that the four large control blades are numbered 1 to 4 in the clockwise direction starting in the lower left quadrant in Fig. 1. Thus, safety Blade 3 -- which was discussed above -- is located in the upper right quadrant in Fig. 1. Finally, this sketch also clearly identifies the location of the beam tubes, the FNI, and the large graphite thermal column relative to the core layout.

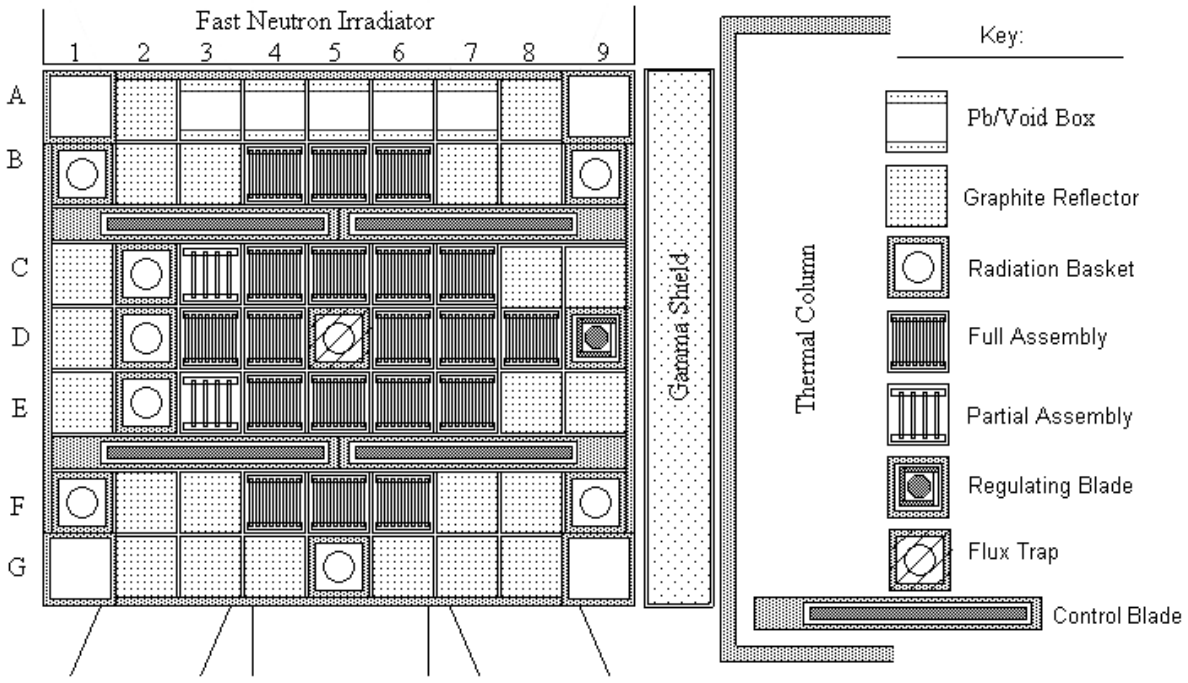

Fig. 1 Rough sketch of the M-2-5 core configuration for the UMLRR.

The M-2-5 core has the graphite radiation basket in the D5 flux trap location. However, as noted previously, this element is not currently available because of excessive swelling of the aluminum can that contains the graphite filler material. Since mid-May 2015 the M-2-7 core, with a

graphite reflector in location D5, is serving as a temporary replacement until a more permanent solution is found. The options for an experimental basket assembly in this location are limited to three design choices, which differ only in the choice of material -- graphite, water, or aluminum -- that occupies the region between the inner Al tube (where the experimental bayonet can be inserted) and the outer Al can.

Graphite Radiation Basket (GRB): This element design is reference and it has been in use within the M-2-5 core since the conversion to LEU fuel in Aug. 2000 until recent events in May 2015 when excessive swelling of the outer aluminum can was noticed. The graphite design was originally selected since it minimized power peaking in the nearby fuel relative to a regular water-filled radiation basket. One option for regaining access to this experimental facility, of course, is to identify the cause of the swelling and to have a new graphite element made that addresses the issue while retaining similar neutronics characteristics.

Water Radiation Basket (WRB): One immediate option that could restore the experimental facility in the central D5 position is to place an existing water radiation basket in this location. This option is not ideal since it increases the local power peaking in the nearby fuel elements and it has a relatively large reactivity effect on the core. However, of most concern is the large positive worth associated with insertion of an experimental bayonet into D5 for the WRB design, which is roughly 3-4 times that seen in the reference design. It should be noted that, because D5 represents a high worth location, no movable experiments are allowed in this position. Thus, any reactivity adjustments that may be needed due to a fixed experiment in D5 can certainly be balanced with a lower critical position on startup. However, for routine operation, it is advantageous to keep the variation in critical blade heights between startups to a minimum, if possible. Thus, although a WRB in D5 is feasible, it is not ideal from an operational perspective.

Aluminum Radiation Basket (ARB): An alternate choice for a suitable material that retains many of the positive features of the GRB is to use aluminum instead of graphite within the assembly that is placed in the D5 flux trap position. Aluminum has a slight negative reactivity effect relative to graphite, but this can be easily compensated by other adjustments (such as replacing the partial fuel elements with full fuel). However, aluminum tends to reduce the flux peaking seen in the neighboring fuel elements similar to graphite and it also has bayonet worth effects similar to graphite -- and it may be a less expensive option and have smaller lead times relative to the manufacture of a new graphite radiation basket (GRB). Thus, a solid aluminum radiation basket (ARB) with a central hole for experimental purposes also appears to be a viable option.

To substantiate some of the above comments/statements, a series of calculations were performed to evaluate the relative merit of the above options, with the M-2-5 core with the GRB in D5 as reference. Because of the negative reactivity associated with the extra water and aluminum relative to graphite, the WRB and ARB options in D5 require some reactivity compensation, so the two partial fuel elements in C3 and E3 were replaced with full fuel elements to maintain sufficient excess reactivity within the core. With this change, the key reactivity, flux, and peak power density results for the various options are compared in Table 4. As apparent, the water radiation basket (WRB) option gives the largest experimental thermal flux, but it also has the largest peak power density and the largest positive worth of a dry bayonet in D5, both of which are negative attributes. In contrast, although the aluminum radiation basket (ARB) gives a slightly lower peak thermal flux by about 15% relative to reference, the peak power density in the nearby fuel is also reduced and it has a comparable bayonet worth to the reference M-2-5

core configuration. Finally we note that balancing reactivity effects of the WRB and ARB options with the replacement of the two partial fuel elements with full fuel assemblies is a positive feature, since this tends to reduce the left-to-right flux distribution asymmetry a little, resulting in a somewhat more balanced reactivity worth distribution among the four large control blades. In summary, it appears that all three flux trap options are feasible, but that the graphite or aluminum options are preferable over the water basket design because of the higher peak power density and the larger worth associated with the placement of an experimental bayonet in the D5 position that is observed with the WRB option.

Table 4 Relative comparison of various flux trap options in the D5 position.

Model Description	**Reactivity Change** %Δk/k from M-2-5	**Worth of Dry Bayonet** %Δk/k	**Peak Thermal Flux** neutrons/cm^2-s		**Peak Power Density** W/cm^3
			No Bayonet	**With Bayonet**	
M-2-5 with GRB in D5	---	0.15	3.5e13	2.0e13	45.0
M-2-5 with full fuel in C3 & E3 and WRB in D5	-0.23	0.57	4.4e13	3.2e13	49.0
M-2-5 with full fuel in C3 & E3 and ARB in D5	+0.11	0.15	3.2e13	1.7e13	41.0

Thus, for the current safety analyses, the M-2-5 core will remain as the reference configuration, even though the existing graphite radiation basket is not in service. Depending on availability and cost, the current plan is to either replace the damaged GRB with a new one or to purchase an aluminum radiation basket (ARB) as a substitute. However, although not the best option from routine operational considerations, we would like to keep the use of the water radiation basket (WRB) as a viable future alternative for special applications (i.e. where high thermal fluxes are needed or for various educational exercises/demonstrations), so the safety analyses described later in this report include the larger peaking factor that is associated with the WRB option. Since the WRB design for the D5 flux trap position gives the worst-case peaking factors, using this case to establish an upper bound gives the UMLRR maximum flexibility in future operations.

In closing this subsection, we note that the control model in the reference M-2-5 model uses the original FSAR description of the four large control blades (as discussed above). Some of our recent computational models use the new BORTEC MMC geometry and material composition but, as also noted above, the differences seen in the different control models are relatively small. Also, once a new experimental basket assembly becomes available -- probably the new aluminum radiation basket (ARB) design -- and the remaining three MMC control blades are installed, the “new” reference core design will certainly include all these features. However, even here, it is expected that the “new” reference configuration will have similar characteristics

to the original M-2-5 core that has been in operation for the last 13 years or so. Thus, the M-2-5 layout makes a perfect reference core for the safety analyses. Finally, since the largest peaking factors occur at the critical beginning-of-life (BOL) state, the reference case has the blades positioned at 14.9″ withdrawn to represent the actual UMLRR M-2-5 BOL critical configuration.

IV. Computer Codes and Model Validation

The physics calculations performed as part of this work include 3-D UMLRR models in both the VENTURE diffusion theory code[14] and MCNP Monte Carlo code.[15] The two-group cross sections for VENTURE are generated using a variety of modules from the SCALE package.[16] In general, VENTURE is used to obtain the power and few-group flux distributions within the UMLRR and for most routine reactivity evaluations involving blade worth distributions, excess reactivity evaluations, etc.. In addition, VENTURE is used for most of the depletion analyses performed to date. Note, however, that burnup effects within the UMLRR are relatively minor since the accumulated burnup is so low (only about 70 MWD in about 13 years of operation of the LEU core). Thus, for most applications, a BOL model with fresh fuel compositions is used with the blade positions adjusted to account for the current critical height (the critical height in the BOL M-2-5 core was about 14.9″ withdrawn and, after about 70 MWD, it was about 16.9″).

In contrast, the MCNP code is used for general validation purposes, for evaluation of specific detailed experiments, and for certain studies where the VENTURE model has known deficiencies. For example, the VENTURE model predicts a small negative worth associated with a dry experimental bayonet inserted into the D5 flux trap position, whereas the MCNP model predicts a positive worth that is reasonably consistent with measure data. Thus, the MCNP model was certainly better suited for the recent comparative analysis of the GRB, WRB, and ARB design options for the D5 flux trap position (as discussed above).

Overall, however, the combined use of both the VENTURE and MCNP models give a good representation of the physics behavior of the UMLRR, and ample evidence has been accumulated over the years that support our confidence in these tools. In particular, Refs. 17-19 give lots of detail concerning both the 3-D VENTURE and MCNP models, along with several inter-comparisons and evaluations relative to actual measured data for the UMLRR. In most cases, the results are quite satisfactory and they certainly support the use of these computational models as part of the current safety analyses.

Concerning the safety analysis, the majority of the thermal calculations was completed using three computer codes -- NATCON, PLTEMP, and PARET-ANL -- that are suitable for the analysis of plate-type fuel operated in a low-pressure environment. This set of codes[20] was originally obtained for use in the UMass-Lowell HEU to LEU conversion project from the RERTR group at Argonne National Laboratory (ANL) back in 1988, and a newer version was obtained in late 1999 to support a preliminary study that looked at the possibility of upgrading the UMLRR to the 2 MW level.[21] More recently, however, a 2001 version of PARET-ANL was obtained from the Radiation Safety Information Computational Center.[22] For future reference, the 1999 versions of NATCON and PLTEMP were used to do the steady-state studies, and the 2001 version of PARET was used to do all the transient analyses as part of the current work.

To give a brief summary of the codes, NATCON is a relatively simple natural convection steady state analysis tool that is used to simulate the conditions of natural convection flow in a thin rectangular fuel channel. For a given power level, it balances buoyancy and friction forces to determine the steady state flow rate in the channel for the given heat source and, for this work, it

was used to find the power level at which the onset of nucleate boiling (ONB) occurs under steady state natural convection conditions. Similarly, PLTEMP also models a steady state system, but it assumes forced convection flow instead of natural convection. The PLTEMP code was used to simulate pump flow through the entire reactor core to determine the amount of flow in the fuel vs. the bypass channels (control regions, experimental basket elements, etc.). In addition, it was also used to do a hot channel analysis to determine the thermal characteristics of the fuel, clad, and coolant as a function of power level and flow rate -- all at steady state forced flow conditions. The hot channel analysis in PLTEMP was used to determine a power-to-flow map to identify, at a given power level, what flow rate would lead to ONB conditions.

PARET-ANL (or just PARET for short), in contrast, is a transient analysis code that can simulate the behavior associated with both reactivity and flow-induced transients within the system. In particular, for the current work, PARET was used to evaluate the consequence of both rapid and ramped reactivity changes in the reactor core, and to determine how a loss of flow scenario affects reactor performance and safety. The PARET analysis was used to show that ONB conditions would not be reached under a series of limiting credible reactor transients.

Unfortunately, the UMLRR does not have any devices that give a direct measurement of the temperatures that develop within a fuel channel -- thus, direct validation of the results from NATCON and PLTEMP is not possible. However, during transient operation, the power level, P(t), is recorded and, using a recently-developed inverse kinetics technique,[23] the total core reactivity, $\rho(t)$, can also be measured. Thus, with this information, some formal testing of the PARET model can indeed be performed. In particular, a recent set of PARET benchmark tests were performed with the goal of validating the base PARET model and a set of reactivity coefficients that will be used within subsequent PARET safety analyses.[24] The reactor conditions and both the simulated and measured results are discussed in detail in Ref. 24 and, in general, the PARET simulations for the series of reactivity and flow transients studied here show very good overall performance. As an illustration, Figs. 2 and 3 show two particular test cases: a low-power (feedback-free) reactivity transient that tests the base PARET model and basic kinetics parameters used within PARET's point kinetics model, and a natural convection test where the temperature feedbacks are now important. As apparent, these results show that the PARET model can indeed simulate actual reactor behavior with reasonable accuracy -- clearly, in both cases, the P(t) and $\rho(t)$ behavior are well-represented with the PARET simulations.

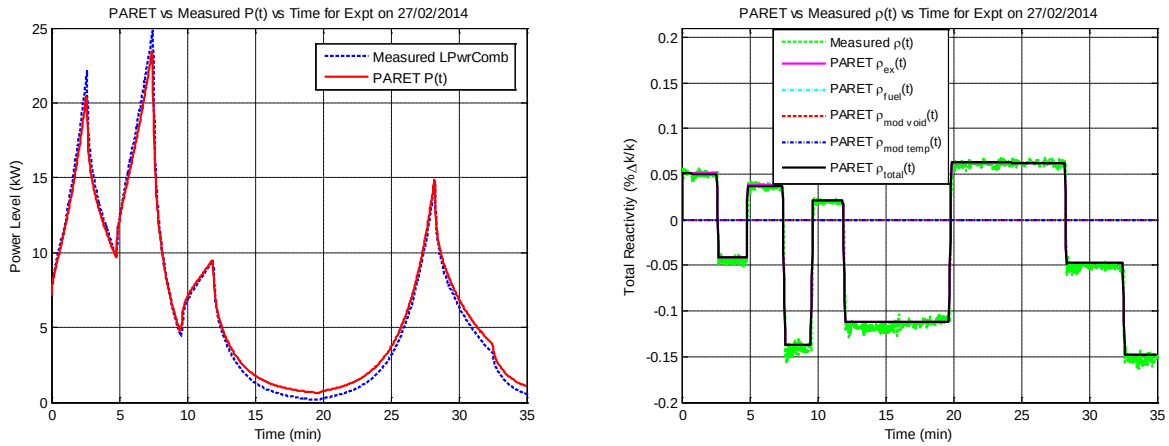

Fig. 2 Summary PARET results for the feedback-free reference test (see Ref. 24).

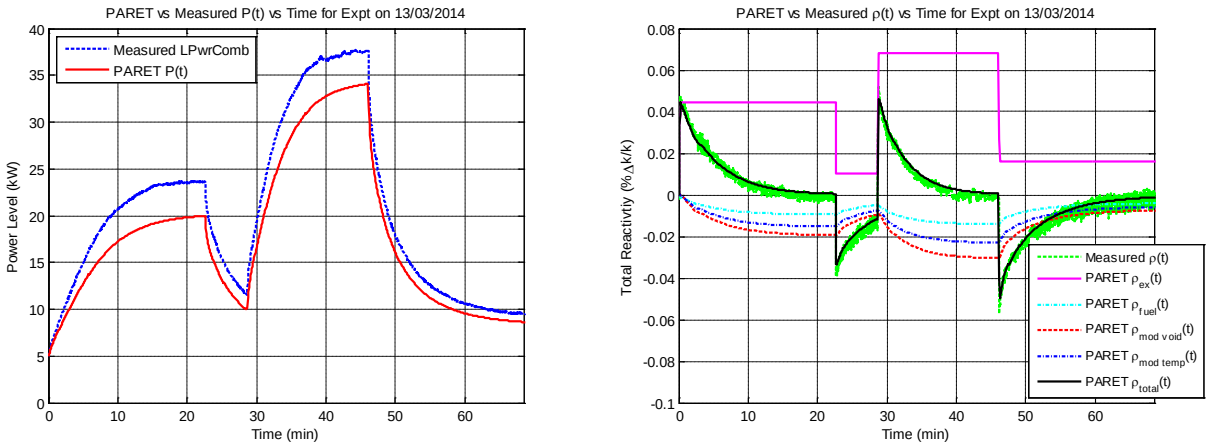

Fig. 3 Summary results for a natural convection test case (see Ref. 24 for details).

V. Reference Parameters for the Safety Analyses

With a set of reasonably accurate physics and thermal analysis tools and models well established, we can now focus on the actual safety studies that were performed. The safety analyses for a particular reactor design typically involve a series of calculations that model the behavior of the system under a series of off-normal conditions to show that fuel integrity will not be compromised under any credible scenario. These computer analyses require lots of modeling data such as the worst-case power peaking factors and axial power distribution, appropriate basic kinetics data and reactivity feedback coefficients, blade worth distributions and drop times (including instrument delay times), typical fluid flow rates and pump-on and pump coast-down characteristics, as well as standard operational conditions at the beginning of a particular transient scenario (such as power level, inlet temperature and pressure, prior operating conditions for decay heat considerations, etc.). This section will briefly discuss and tabulate many of the needed parameters for the subsequent analyses -- however, the reader is encouraged to consult the appropriate references to several other documents/studies for more details, as needed.

V.1 Peaking Factors and Axial Power Profile: From our previous physics studies, we know that the more severe power peaking condition is associated with the blades inserted substantially into the core. Thus, an arrangement with a high excess reactivity which is made nearly critical via blade insertion often gives the desired limiting peaking factors. In particular, the excess reactivity in the BOL M-2-5 was about 3.5 %Δk/k and, although less than the maximum allowable excess of 4.7 %Δk/k, this is sufficiently large enough for extended operation of the UMLRR. Thus, the BOL M-2-5 model with the blades at their critical height of about 14.9″ withdrawn was selected as a good candidate configuration for determining the maximum peaking factors.

It should also be noted that a practical lower limit on excess reactivity is somewhere in the range of 1.5-2.0 %Δk/k, since sufficient excess reactivity is needed to override temperature and xenon feedbacks, to allow for additional fuel burnup, and to the counter negative reactivity effects of experiments. In addition, a minimum shutdown margin of 2.7 %Δk/k also limits the asymmetry that can be allowed in the blade worths, since the shutdown margin is computed with the most reactive blade in its least reactive position (i.e. withdrawn). Thus, all these conditions tend to constrain the allowable configurations that can be realized in practice.

Finally, the maximum peaking factors are strongly affected by the design of the experimental element that is placed in the central D5 flux trap location. As already noted, the water radiation basket (WRB) design gives the largest thermal fluxes and flux gradients, leading to the highest peaking factors in the nearby fuel elements. Although a WRB in D5 is not the best option for routine operation, we want to keep this option available if needed for a specific experiment, so the WRB design was selected for determining the worst case situation.

Within these considerations, the 3-D VENTURE model was used to evaluate a variety of core configurations containing all UMLRR fuel, all WPI fuel, and a mix of both fuel types. In addition, fresh cores and cores with some accumulated burnup were also addressed, again with the goal of addressing as wide a range as possible of practical configurations in order to find a reasonable upper limit for both the radial and axial peaking factors.

Of the many feasible configurations investigated (see Ref. 25 for more details), the worst case core layout that was identified included a BOL 21-element core with the blades at 14.9″ out, a WRB in D5, eight (8) fresh UMLRR uranium silicide elements immediately surrounding the D5 position (i.e. the inner ring of fuel) and, to emphasize the power peaking in the inner ring, the remaining thirteen (13) elements in the outer ring contained the less reactive WPI uranium aluminide fuels assemblies. Although rather contrived, this is a feasible configuration and it had the largest computed peak power density, with a radial peaking factor of $f_{xy} = 1.993$ and an axial peaking factor of $f_z = 1.383$. With these values as a base, it was recommended that these peaking factors both be increased by 5% and rounded up to obtain two significant figures for the quoted values of f_{xy} and f_z. This approach adds some conservatism and gives recommended worst-case peaking factors of about $f_{xy} = 2.1$ and $f_z = 1.5$. These values, which combined leads to a total peaking factor of over 3.1, are the peaking factors used in our subsequent NATCON, PLTEMP, and PARET safety analysis calculations.

To be specific about the axial power prolife, the fuel element in location B5 in the reference M-2-5 core has an axial peaking factor of approximately 1.50 -- thus the axial power distribution in this location was selected for use in the thermal analysis codes. In the code models, 20 discrete axial intervals are used (21 points), so the VENTURE calculated profile was normalized and then interpolated to the 21 points used within the thermal codes, as shown in Fig. 4. This axial profile was used for all the subsequent thermal calculations. For an average channel, the values shown in Fig. 4 were used as displayed. However, for a hot channel analysis, the values shown were multiplied by the radial peaking factor, $f_{xy} = 2.1$, to represent the axial profile in the hottest channel in the core.

V.2 Basic Kinetics Data and Reactivity Coefficients: The PARET code uses the point kinetics approximation, along with a set of reactivity coefficients to treat the inherent temperature feedback effects, to model the transient power and reactivity behavior during the off-normal transient scenario being simulated. One common form of the point kinetics equations can be written as

$$\frac{dT}{dt} = \frac{(\rho - \beta)}{\Lambda} T \quad + \quad \sum_i \lambda_i c_i \quad + \quad q \qquad (1)$$

$$\frac{dc_i}{dt} = \frac{\beta_i}{\Lambda} T \quad - \quad \lambda_i c_i \qquad \text{for } i = 1, 2, \cdots 6 \qquad (2)$$

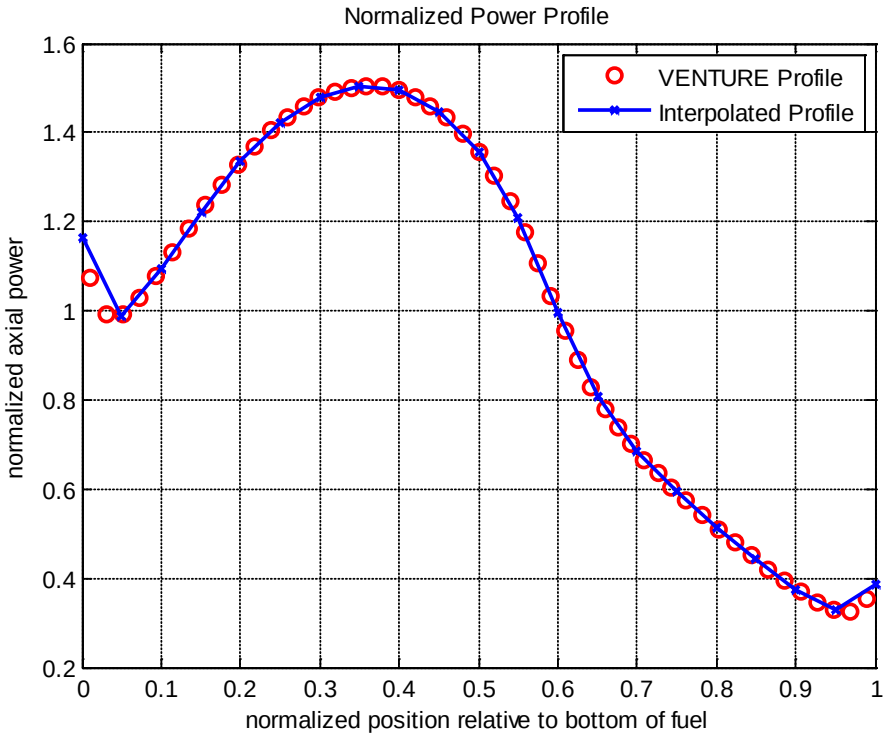

Fig. 4 Normalized axial power profile used in subsequent thermal analysis calculations.

where T(t) and $c_i(t)$ are, respectively, the normalized neutron amplitude and normalized precursor levels, and the quantities, β_i, λ_i, Λ, and $\beta = \Sigma\beta_i$,, are referred to as the kinetics parameters (where β refers to the effective delayed neutron fraction, β_{eff}). For application here, the source term, q, is set to zero, the neutron amplitude is replaced by the reactor power, P(t), since the two quantities are proportional, and the kinetics parameters are treated as constants for a particular reactor design. The total reactivity, $\rho(t)$, includes both the external reactivity, $\rho_{ex}(t)$, that is under operator control via control blade movement, and the compensated or feedback reactivity, $\rho_c(t) = \rho_f(t)$, that is due to inherent temperature changes in the system. In PARET, the feedback reactivity components are represented in the form of reactivity coefficients multiplied by a change in the parameter of interest (fuel and moderator temperature and moderator %void). Thus, the feedback reactivity, in dollars, is given as

$$\rho_f(t) = \alpha_{Tf}\left\{T_f(t) - T_{f_{ref}}\right\} + \alpha_{Tm}\left\{T_m(t) - T_{m_{ref}}\right\} + 100\alpha_V\left\{V_m(t) - V_{m_{ref}}\right\} \qquad (3)$$

where the reactivity coefficients, α_{Tf}, α_{Tm}, and α_V for the fuel temperature, moderator temperature, and moderator void, respectively, are given in either \$/^oC or \$/%void. More complicated expressions are available to account for the temperature dependence of the reactivity coefficients, but the current PARET models of the UMLRR assume that these are relatively constant, so this additional detail is not used at present.

The kinetics parameters used for the PARET safety studies are the same ones used since the early 1990s during the initial HEU to LEU conversion studies[26] and these are summarized in Table 5 for future reference. The RERTR program at ANL computed the generation time and

β_{eff} values shown here,[27] and the decay constants and the delayed neutron distribution among the six precursor groups were derived from ENDF/B-V data.[28] The good comparisons shown in Fig. 2 were generated within PARET using the kinetics data from Table 5 -- thus, these data will continue to be used since they appear to be well-suited for use with the current UMLRR PARET models.

Table 5 Point kinetics data used in the UMLRR PARET models.

βeff	**0.0078**		**Λ (μsec)**	**65**
Precursor Group	**Precursor Weights β_i/β_{eff}**		**Decay Constants λ_i (sec^{-1})**	
1	0.038		0.0127	
2	0.213		0.0317	
3	0.188		0.1160	
4	0.407		0.3111	
5	0.128		1.400	
6	0.026		3.871	

However, it should be noted that an attempt was made to use the latest UMLRR MCNP model to generate updated values for the kinetics parameters, but the values generated in that effort gave relatively poor results relative to the reference data from our early work as shown in Table 5. In particular, relatively good comparisons from the feedback-free test case displayed in Fig. 2 were generated with the old data, but the comparisons with the new MCNP kinetics parameters were rather poor. Since the benchmark results for the feedback-free test case were so good using the old data set, the issue with the new MCNP-generated kinetics parameters was not pursued any further at this time (this may be addressed further at some later time).

Concerning the feedback coefficients, Michael Pike generated a complete set of these data as part of his MS thesis work a few years ago.[29] And, as part of our current effort to validate the PARET model for the UMLRR, including the reactivity coefficients, the raw data generated by M. Pike were re-evaluated and a new slightly modified set of coefficients were derived. The resultant coefficients developed in this re-evaluation are summarized in Table 6 and these were the values used in the full benchmark analysis documented in Ref. 24 -- with partial results illustrated in Fig. 3 shown above. For specificity, the values in bold in Table 6 were the ones used in the PARET input file, with the unit of reactivity in dollars ($), and these correspond to the three reactivity coefficients needed within eqn. (3). However, it should be noted that, for added conservatism for the subsequent "worst-case" transient studies to establish the safety limits, it was decided to modify the coefficients in Table 6 in a conservative manner by 25% to account for any uncertainties that may exist in both the models and their input reactivity coefficient information. Thus, the magnitude of the PARET input values in the safety analysis runs are 25% lower or 25% larger, as appropriate, than those in Table 6.

A final point here, that is emphasized in more detail in Ref. 24, is that the computed and measured isothermal temperature coefficients, $\alpha_{ITC} = \alpha_{Tcoolant} + \alpha_{Tfuel}$, for the UMLRR at room temperature differ by more than a factor of two. In fact, this inconsistency is what initially

prompted the detailed validation effort reported in Ref. 24. Unfortunately, however, the benchmark study did nothing to resolve the issue, but it did show, without doubt, that the computed values of the reactivity coefficients as given in Table 6 lead to very reasonable results for the PARET simulations for a variety of transient situations -- and that a reduction in magnitude by more than a factor of two is not justified. Thus, based on the positive results of the validation tests as discussed in Ref. 24, we have decided to set aside this unresolved issue for now, and move forward using the new nominal reactivity coefficients listed in Table 6 in all future best-estimate studies using the PARET code.

Table 6 New reactivity coefficient evaluation for the M-2-5 BOL core (β_{eff} = 0.0078).

Component	Reactivity Coefficients	
Water Temp Only	**-5.30e-5 Δk/k/°C**	**-6.79e-3 $/°C**
Water Density Only	-6.91e-5 Δk/k/°C	-8.86e-3 $/°C
total $T_{coolant}$	-1.22e-4 Δk/k/°C	-1.56e-2 $/°C
T_{fuel}	**-2.12e-5 Δk/k/°C**	**-2.72e-3 $/°C**
$T_{coolant}$ + T_{fuel}	-1.43e-4 Δk/k/°C	-1.83e-2 $/°C
Coolant Void	**-2.59e-3 Δk/k/%void**	**-3.32e-1 $/%void**

V.3 Blade Worth Distribution and Drop Times: When performing both reactivity-induced and flow-induced transient simulations in PARET, the user has an option to scram the reactor on either a high-power signal or a low-flow indication. This capability models the safety blades being de-energized and dropping rapidly into the core -- thus "scramming the reactor" and causing the power level to drop rapidly. This simulation scenario in PARET assumes some delay time from when the preset scram limit is reached to when the magnets de-energize, and then the blades drop into the core using a user-specified blade speed and blade worth curve.

The UMLRR Technical Specifications say that the total drop time must be less than 1 second from a fully withdrawn position, which includes the instrument delay time and the physical time to drop by gravity through the approximately 25-inch length of the blade. This capability must be verified annually. The actual measurement is taken from full-out to about 4 inches withdrawn because of the physical location of the sensors (but the lower 4 inches only account for about 4-5% of the total blade worth anyway). Using the total 1-second requirement as the actual travel time gives a minimum average blade speed of (25 - 4) inches/sec = 0.533 m/sec, and this is the value used in the PARET input for the safety calculations. This value is conservative because the usual measured total drop time includes the instrumentation delay as well as the physical travel time, and these combined times are always less than the 1-second limit.

As noted above, PARET treats the instrument delay as a separate time interval, during which no blade movement occurs. In practice, this delay time is a very important quantity in the overall simulation, since as soon as the blades start to drop, the transient power and temperatures very quickly start to fall. This delay time was estimated many years ago and a value of 280 msec has been used since the early 1990s -- for example, a delay time of 280 msec was used within the step reactivity simulations that were part of the safety analysis calculations for the FSAR Supplement for Conversion to LEU Fuel.[26-27] However, in early Aug. 2015, a fast data logger

was purchased so that the time it takes to de-energize the magnets could be measured as accurately as possible -- and all the measured delay time values were very nearly 185 msec.[30] Thus, with some added conservatism (nearly 15%), 210 msec is used in the subsequent PARET safety computations for the instrument delay time.

For the blade worth curves that are input to PARET, the assumption is made that the reactor is critical with the blades at roughly 15 inches withdrawn and that, for some unspecified reason, the electromagnet for Blade 4 (which has the largest worth) does not de-energize -- thus, only Blades 1-3 drop into the core after the specified delay time following a scram signal. The Jan. 2015 blade worth curves for the M-2-5 core were used to collect data at 1-inch intervals starting at 15 inches withdrawn. The inserted worths for Blades 1-3 were summed and both the position and reactivity were converted into proper units for use in PARET. The results of these manipulations are summarized in Table 7, with the last two columns representing data actually input to the code. Whenever a scram occurs, the average blade speed (0.533 m/s) coupled with the worth vs. distance inserted data in Table 7 are converted into reactivity vs. time and used as the external reactivity component, $\rho_{ex}(t)$, for the particular transient under study.

Table 7 Blade worth vs. insertion distance for PARET input file.

Inches Withdrawn	Inserted Worth (%Δk/k)	Inserted Worth ($)	Distance Inserted (m)
15	0.000	0.00	0.000
14	-0.539	-0.69	0.025
13	-1.109	-1.42	0.051
12	-1.693	-2.17	0.076
11	-2.274	-2.92	0.102
10	-2.836	-3.64	0.127
9	-3.363	-4.31	0.152
8	-3.842	-4.93	0.178
7	-4.262	-5.46	0.203
6	-4.618	-5.92	0.229
5	-4.905	-6.29	0.254
4	-5.126	-6.57	0.279
3	-5.285	-6.78	0.305
2	-5.390	-6.91	0.330
1	-5.454	-6.99	0.356
0	-5.487	-7.03	0.381

V.4 Pump-On and Pump Coast-Down Characteristics: Two flow transients that need to be analyzed as part of the overall safety analysis include a pump-on "cold water insertion event" and a pump-off "loss-of-flow scenario." Particular versions of both of these events were analyzed as part of the validation tests documented in Ref. 24. These tests, however, were

performed under a set of rather mild and specialized operating conditions so that the reactor would not hit (or even come close to) any of its limiting conditions (i.e. so it would not scram). In contrast, during normal forced flow operation, for example, if the primary pump suddenly fails, the flow rate will decrease quickly in an exponential-like fashion, and a reactor trip will be triggered when the flow rate reaches the low-flow setpoint. Similarly, if the primary-pump is inadvertently turned on during natural convection operation, the power increase due to the positive reactivity insertion following the rapid addition of colder water in the core will undoubtedly cause the reactor power to exceed its natural convection limit of 125 kW, which again would scram the reactor. To formally simulate both these scenarios in PARET, the pump characteristics need to be known following both a pump-on and pump-off event.

In particular, to simulate the pump-off and pump-on sequences in PARET, we need to have information concerning the pump coast down and startup curves. In 2011, a series of pump-off and pump-on tests were performed and the resultant "pumps curves" were analyzed in some detail. Specifically, for a pump-on event, the pump approaches full capacity very rapidly (in about 2 seconds) and this is modeled in PARET as a simple ramp function that goes from zero flow to full flow in 2 seconds. For the pump-off scenario, the pump coast down is more gradual, occurring over a period of about 10 seconds. On March 3, 2011, a series of four pump-off events were recorded and, from the measured flow rate data, an average coast-down curve was obtained as shown in Fig. 5. Numerical data from this curve was extracted at 1-second intervals to give:

Time (secs)	0.0	1.0	2.0	3.0	4.0	5.0	5.0	7.0	8.0	9.0
Flow Fraction	1.000	0.923	0.551	0.316	0.194	0.138	0.107	0.084	0.057	0.044

The data from this table are used within PARET to represent the fraction of full flow following a pump trip, with the value set to exactly zero for $t \geq 10$ seconds.

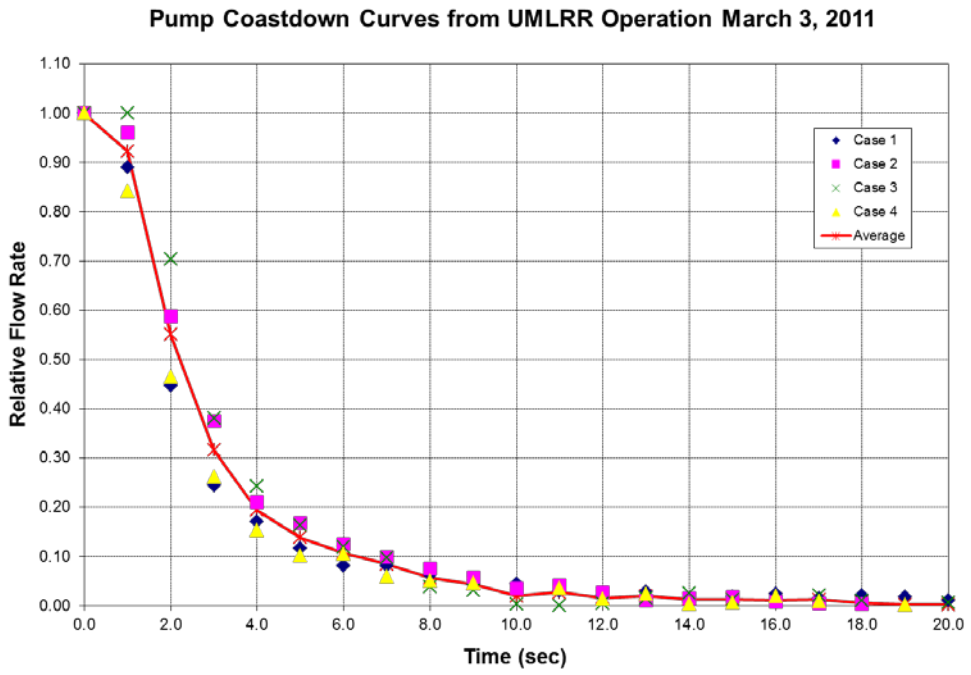

Fig. 5 Pump coast-down curve for the UMLRR primary pump.

V.5 Flow Distribution and Assembly Flow Rates: When operating in forced flow mode with the primary pump on, the coolant flows downward through the core with a nominal pump flow rate of about 1700 gpm. In steady state, a pressure drop (ΔP) across the core is established due to wall friction, inlet/exit effects, and elevation changes and, because of mixing in the common inlet and outlet plena, the same ΔP is imposed across each fuel and bypass channel. If one imposes a specific ΔP across the core, the flow rate in all the individual channels (fuel, control elements, radiation baskets, etc.) can be determined, summed, and finally, the relative flow distribution (i.e. fraction of total flow in each region) can be found.

Full core models within PLTEMP for various core sizes (i.e. number of fuel assemblies) were generated for the sole purpose of finding the fraction of pump flow that is expected per fuel element. These models were relatively detailed geometrically, with three axial regions for determining pressure drop in the fuel channels and three different bypass channels (radiation baskets, control blades, and regulating rod) to account for nonfuel flow. Because of the different fuel channel sizes, calculations were performed separately for the UMLRR U_3Si_2-Al fuel elements and for the WPI UAl_x-Al fuel assemblies.

The information needed for these types of calculations includes the flow area, hydraulic diameter, region length, and entrance and exit loss coefficients for each axial region for each element type. There are four assembly types in the model: N fuel assemblies, where N varied from 20 to 26 fuel elements, and three types of bypass regions including five radiation baskets, four large control blades, and one regulating blade. A maximum of five open radiation baskets can be present in the core at one time to limit the amount of bypass flow (and to assure that there is sufficient flow in the fuel channels). Finally, it should also be noted that flow on the outside of the assemblies was assumed to be negligible, since the bottom grid plate blocks direct downward flow – with essentially zero flow area.

With knowledge of the flow regions and various assumptions concerning the loss coefficients associated with the entrance and exit effects of each axial region for the fuel and bypass regions, PLTEMP was able to compute the flow distributions that can be expected in both the UMLRR and WPI-fuelled cores. These calculations were performed for several power level and core ΔP specifications, and the actual relative flow distributions were found to be essentially independent of both power and total flow. Finally, as an upper bound on the fuel element flow fraction, the flow distribution was computed based solely on minimum flow area. This latter computation represents an upper estimate of the fraction of flow in the fuel region because the fuel channel generally has the largest wall friction and loss coefficient components -- which will result in a ΔP common to the other bypass channels only if the flow rate is lower relative to the bypasses with less friction loss.

A summary of the results from the above computations is given in Tables 8 and 9. In particular, Tables 8a and 8b show the minimum flow area distribution for both the UMLRR and WPI fuel elements, respectively, as a function of the number of fuel assemblies present in the core. These data clearly show that, based on only flow area, one would expect that roughly 77% – 82% of the total pump flow would go through the fuel elements, with slightly less flow in the WPI vs. UMLRR fuel because of the somewhat smaller channel dimensions in the WPI element design (see Table 1 on page 3). However, knowledge of the total flow area, by itself, does not tell the whole story since it ignores the friction loss differences in the different channels, which is clearly greater in the small fuel channels with their associated wall surface friction and larger contraction and expansion losses at the entrance and exit of each channel. The PLTEMP

calculations take these friction effects into account and the summary comparisons are given in Table 9. Clearly, the importance of the increased friction in the fuel channels is obvious -- and it leads to a significant decrease in core flow (i.e. fraction of flow in the fuel channels) relative to that estimated from a simple analysis of flow areas.

Table 8a Normalized flow areas by element type with UMLRR fuel.

	Normalized Flow Areas for UMLRR Fuelled Core				
# Fuel Assemblies	**Fuel Elements**	**5 Radiation Baskets**	**4 Large Control Blades**	**1 RegBlade**	**Total**
20	0.783	0.093	0.113	0.011	1.000
21	0.792	0.090	0.108	0.010	1.000
22	0.799	0.087	0.104	0.010	1.000
23	0.806	0.084	0.101	0.009	1.000
24	0.813	0.081	0.097	0.009	1.000
25	0.819	0.078	0.094	0.009	1.000
26	0.825	0.076	0.091	0.009	1.000

Table 8b Normalized flow areas by element type with WPI fuel.

	Normalized Flow Areas for WPI Fuelled Core				
# Fuel Assemblies	**Fuel Elements**	**5 Radiation Baskets**	**4 Large Control Blades**	**1 RegBlade**	**Total**
20	0.771	0.099	0.119	0.011	1.000
21	0.779	0.095	0.115	0.011	1.000
22	0.787	0.092	0.111	0.010	1.000
23	0.794	0.089	0.107	0.010	1.000
24	0.801	0.086	0.103	0.010	1.000
25	0.808	0.083	0.100	0.009	1.000
26	0.814	0.080	0.097	0.009	1.000

As noted above, because of the slightly smaller channels, the WPI element design has a smaller portion of the total flow through the fuel region by roughly 1-2% relative to the original UMLRR LEU fuel element design. Thus, to be conservative, we focus on the last column of Table 9 to obtain the fraction of fuel flow for both the WPI and UMLRR elements. A simple linear fit through these data gives the following expression

$$f = 0.50 + 0.0088\,N \qquad (4)$$

where f is the fraction of total pump flow that goes through the fuel and N is the number of fuel elements in the core.

Table 9 Fraction of flow in the fuel channels with and without friction losses.

	UMLRR Fuelled Core		WPI Fuelled Core	
# Fuel Assemblies	**Based only on flow areas**	**PLTEMP calculation with friction losses**	**Based only on flow areas**	**PLTEMP calculation with friction losses**
20	0.783	0.688	0.771	0.677
21	0.792	0.705	0.779	0.689
22	0.799	0.714	0.787	0.699
23	0.806	0.722	0.794	0.708
24	0.813	0.732	0.801	0.716
25	0.819	0.740	0.808	0.724
26	0.825	0.746	0.814	0.730

For the reference 21-element M-2-5 core, for example, eqn. (4) says that about 68.5% of the nominal 1700 gpm flow rate goes through the fuel elements. Since flow in the bypass regions (radiation baskets and control elements) is not modeled explicitly in the safety calculations, eqn. (4) is used to relate the total pump flow rate, Q_{pump}, to the flow rate through the fuel elements, Q_{assy}, and individual fuel channels, Q_{chan}, or

$$Q_{assy} = \frac{\text{flow rate in all fuel}}{\text{number of assemblies}} = \frac{Q_{pump} \times f}{N} \qquad \text{and} \qquad Q_{chan} = \frac{Q_{assy}}{18} \tag{5}$$

where we have used the fact that both the UMLRR and WPI elements have 18 plates and 18 "effective" coolant channels per assembly. Note that, although there are only 16 fuel plates in the UMLRR element, the additional two aluminum edge plates give 18 total plates. Also, with 18 plates, there are really 19 channels -- however, the two edge channels only have half the width of an interior channel, so together, they make up a single channel, giving 18 "effective" coolant channels.

Within the current context, it is convenient to have a conversion factor that relates a single assembly or single channel mass flow rate, w, in kg/s (as used by the codes) to the measured total pump volumetric flow rate in gallons/minute or gpm (as recorded by the reactor instrumentation system). Since the water density change over the range of normal operating temperatures is small, we assume a constant value of 998 kg/m^3 in determining the desired conversion factor, as follows:

$$w_{assy} = Q_{assy}\rho = \frac{f}{N} \times Q_{pump} \left(\frac{gal}{min} \right) \times \frac{1\,min}{60\,sec} \times \frac{1\,m^3}{264.2\,gal} \times 998 \frac{kg}{m^3} = \frac{0.0630\,f}{N} \times Q_{pump}$$

or $$w_{assy} = \frac{0.0630\,f}{N} \times Q_{pump} \tag{6}$$

where Q_{pump} is given in gpm and the assembly mass flow rate, w_{assy}, is in kg/s. For example, for N = 21, the conversion factor in eqn. (6) evaluates to 2.054e-3 kg/s per gpm of pump flow -- or stated differently, Q_{pump} in gpm is 487 times the assembly mass flow rate, w_{assy}, in kg/s for a

21-element core. This latter conversion factor was actually used to convert the assembly flow rates obtained from the PLTEMP code to overall UMLRR primary pump flow rates in gpm.

Another related quantity of interest is the mass flux, w″, which has units of mass flow rate per unit area, or kg/s/m^2. This quantity is useful since it is independent of the entity of interest -- for example, the mass flux in a single channel, in the assembly, or in all N fuel elements is the same value. In particular, PARET needs to know the mass flux in the fuel region to compute the flow velocity, the Reynold's number, the pertinent flow regime (laminar or turbulent), the heat transfer coefficient, and so on.

For convenience, a short tabulation of flow rate information is given in Table 10 for the reference 21 fuel element case for several pump volumetric flow rates of interest. Note that, in particular, the fraction of core flow through the fuel as given by eqn. (4) is the same for both the UMLRR and WPI assemblies (as discussed above). Because of this, channel mass flow rates are the same for the two fuel types for a given number of elements, but the mass fluxes are somewhat different because of the different flow areas within the UMLRR and WPI elements. The values of Q_{pump} given here correspond to typical operational conditions utilized within the last few years (1600, 1650, and 1700 gpm), to the LCO flow rate (1550 gpm), and to the LSSS flow rate (1370 gpm) -- where LCO refers to Limiting Conditions for Operation and LSSS stands for Limiting Safety System Settings. PARET calculations have been performed primarily for these pump flow rates, so Table 10 is included simply for convenience in identifying the specific values of the mass flux used within the code inputs.

Table 10 Coolant flow rate information for a 21-element core.

Q_{pump} (gpm)	w_{chan} (kg/s)	mass flux, w″ (kg/s/m^2)	
		UMLRR fuel	WPI fuel
1700	0.194	9.916E+02	1.068E+03
1650	0.188	9.624E+02	1.037E+03
1600	0.183	9.332E+02	1.005E+03
1550	0.177	9.041E+02	9.738E+02
1370	0.156	7.991E+02	8.607E+02

The last item of interest in this subsection concerns the power-to-flow ratio vs. number of fuel assemblies. Clearly, for a given power level, as the number of elements increases, the power per element or power per fuel plate decreases. Within the same context, the flow rate per element also decreases as the number of elements increases. Thus, the real question of interest is "How does the power-to-flow ratio (i.e. kW/gpm) vary with the number of fuel elements in the core?". This can be expressed in mathematical form as

$$\left.\frac{\text{power}}{\text{flow}}\right|_{\text{ave}} = \frac{\text{ave power per assy}}{\text{flow rate per assy}} = \frac{P_{tot}/N}{\left(Q_{pump}\times f\right)/N} = \frac{P_{tot}}{Q_{pump}\times f} = \frac{P_{tot}/Q_{pump}}{0.50+0.0088\,N} \qquad (7)$$

where the fraction of flow through the fuel, f, as given by eqn. (4), is included directly in the last version of this expression. This clearly shows that, for a given power level and pump flow rate,

the power-to-flow ratio decreases with increasing N. The decrease is slow, only changing from 0.87 kW/gpm to 0.81 kW/gpm over the range from N = 20 to N = 26 for the case of P_{tot} = 1000 kW and Q_{pump} = 1700 gpm. Nevertheless, this suggests that smaller cores are more limiting since the power-to-flow ratio is larger for small N (assuming that the peaking factors do not increase significantly with increasing N, which is not expected and has not been observed in the physics calculations performed to date). Thus, the focus has been on a reference core with N = 21, since this represents a reasonable lower limit for most practical core configurations for the UMLRR, and it also represents a near-limiting arrangement for the safety analyses.

To elaborate a little on the choice of a 21-element reference configuration as a near-limiting arrangement, we note that, with a graphite radiation basket in D5 and three water baskets in C2, D2, and E2 for in-core irradiation applications, 20 fresh fuel elements is the practical minimum number of elements needed for routine reactor operations (for sufficient excess reactivity to overcome temperature effects, xenon reactivity, and to allow for limited burnup). However, to achieve sufficient RegBlade reactivity worth, a fuel element must be in the D8 position. In addition, symmetry considerations and the desire to have high fluxes for experiments placed in the beam tubes as well as in the fast neutron irradiator (FNI), argue for another fuel element (to make 21) to balance the number of fuel elements outside of the control blade regions (i.e. Rows B and F as seen in Fig. 1 on page 6). Finally, considering that the existing fuel has already seen greater than 70 MWD of burnup, it is hard to imagine that there will ever be less than 21 fuel elements in the core for routine operation. From an education and training perspective, many different core configurations are possible (some with less than 21 elements), but these are mostly limited to low power criticality evaluations for demonstration, training, and/or code validation purposes, not for long-term routine operations. Thus, with all these considerations and the fact that smaller tends to be more limiting, the 21-element M-2-5 configuration has been selected as the basis for performing most of the UMLRR safety analyses.

V.6 Engineering Hot Channel Factors: The NATCON and PLTEMP codes were used to establish the steady state operating limits within the LEU fuelled UMLRR during the conversion from HEU to LEU fuel[26,31-32] -- and the same basic procedure has been used as part of this work (with a different radial peaking factor, axial power profile, the inclusion of WPI fuel, etc.). In particular, using PLTEMP, a power vs. flow curve is determined that identifies the relationship of power and overall pump flow rate at which the onset of nucleate boiling (ONB) point is reached. The goal here is to assure that the forced convection steady-state operating point is well within the limits set by this curve. For natural convection operation, NATCON is used to establish the power level where ONB occurs, and again, the nominal operation point is set well below this limit.

In establishing these ONB limits, it is important to take into account the effect of uncertainties in the data and models used in the analysis. In particular, one usually introduces one or more engineering hot channel factors that account for fuel and assembly design tolerances and for uncertainties in various calculated and measured parameters. In NATCON and PLTEMP, these hot channel factors are applied as three separate components,

1. F_q -- accounts for heat flux uncertainties
2. F_b -- treats uncertainties in bulk flow or enthalpy change in a channel
3. F_h -- quantifies the uncertainty in the heat transfer process

These factors (which are greater than or equal to unity) are used to either increase or decrease (as appropriate) the nominal estimate of the heat flux, channel flow rate (which affects the coolant ΔT directly), and calculated heat transfer coefficient. Specifically, each time these quantities are used in the codes, they are modified by the hot channel factors as follows:

heat flux: $q'' = q''_{nom} \times F_q$

mass flow rate: $w = w_{nom} / F_b$

heat transfer: $h = h_{nom} / F_h$

Each of these hot channel factors, in turn, is composed of a number of subfactors. The values of the subfactors are estimated (usually quite conservatively) based on specified design tolerances and experience with various measurement devices and empirical correlations. These subfactors are then combined statistically (usually assuming uncorrelated uncertainties) to give the three factors used within the codes. The only exception to this procedure was for the F_h value, which included the heat transfer coefficient uncertainty as a multiplicative safety factor (see Note 3 in Table 11 below).

The individual values of the subfactors for the UMLRR LEU fuel that were used previously as part of the safety analyses for the UMLRR HEU to LEU conversion effort[26,31] have been reviewed and compared to the values used in the WPI safety analyses[4] performed by the RERTR Program at ANL. In most cases the individual factors were very similar and the resultant values of F_q and F_b were nearly identical as shown in Table 11. As apparent in this comparison, the largest difference in the estimated subfactors was the channel thickness contribution to F_h, where 1.07 was used for the UMLRR fuel and 1.14 was used for the WPI fuel, and this difference resulted in F_h values of 1.35 and 1.41, respectively, for the UMLRR and WPI fuel. Since the underlying assumptions associated with the individual subfactors for the WPI fuel are not available, we decided to go with the values taken directly from the original references without modification (as given in Table 11). Thus, from Ref. 26, the F_q, F_b, and F_h factors used in this work for the UMLRR fuel are 1.25, 1.24 and 1.35, respectively. Similarly, from Ref. 4, the same quantities for the WPI fuel are 1.24, 1.24, and 1.41, respectively. These are the values used in the NATCON and PLTEMP calculations reported below in the section "Steady State Operating Limits".

Before leaving this topic, it should be noted that data and modeling uncertainties are treated differently in the transient calculations, since the PARET code does not include explicit usage of the hot channel factors noted above. Instead, for the transient calculations, very conservative assumptions and initial operating points are used to account for the inherent modeling uncertainties that exist in any simulation of a real system. For example, the heat flux hot channel factor, F_q, accounts for a number of physical and measurement uncertainties that affect the heat flux seen in the real system. In PLTEMP, for instance, one uses a nominal power level as input to the code, but then internally the code multiplies the calculated heat flux (which is directly proportional to the power) by F_q to account for the uncertainties associated with this quantity. In PARET, on the other hand, the user simply inputs a larger value of initial power to account for the inherent uncertainties. For example, nominal full power for the UMLRR in forced flow mode is 1 MW, but the worst-case reactivity-induced transient analyzed has the input power at the LSSS value of 1 MW × 1.25 = 1.25 MW. Similarly, the nominal pump flow rate is 1700 gpm, but the transient calculations are run at the LSSS flow rate value of 1700 gpm / 1.24 = 1370

gpm. These conservative initial conditions plus a high inlet temperature, large peaking factors, and conservative reactivity coefficients, blade worths, instrument delay times, etc., all coupled with ONB as the safety limit, should add a significant real safety margin to more than cover any uncertainties that exist in the system.

Table 11 Hot channel factor data used in both NATCON and PLTEMP computations.

	UMLRR Fuel (from Ref. 26)				WPI Fuel (from Ref. 4)		
Subfactors	**F_q**	**F_b**	**F_h**		**F_q**	**F_b**	**F_h**
Fuel Meat Thickness	1.08	--			1.07	--	
U235 Loading	1.05	1.05			1.02	1.02	
U235 Homogeneity[(1)]	1.20	1.10			1.20	1.10	
Channel Thickness[(2)]		1.15	1.07			1.16	1.14
Power Measurement	1.05	1.05			1.05	1.05	
Calculated Power Density	1.10	1.10			1.10	1.10	
Coolant Flow Rate		1.10	1.10			1.10	1.10
Heat Transfer Coefficient			1.20				1.20
Statistical Total[(3)]	1.25	1.24	1.35		1.24	1.24	1.41

NOTES:

1. F_q corresponds to radial uncertainty, F_b relates to axial uncertainty.
2. A 10% uncertainty in channel thickness was assumed for the UMLRR fuel. The values given for the UMLRR fuel correspond to the worst-case observed uncertainty in ΔT_{water} and ΔT_{clad}, respectively.
3. In general, the total hot channel factor is computed assuming uncorrelated uncertainties. For F_h, the channel thickness and flow rate factors are combined statistically and the heat transfer component is treated as a multiplicative (safety) factor.

VI. Steady State Operating Limits

For safety-related studies, one needs to establish some limiting criteria that will guarantee safe operation of the reactor at all times. As mentioned previously, for the UMLRR, the limiting criteria for both steady state operation and for credible off-normal protected transients is the onset of nucleate boiling (ONB) point. Since the coolant saturation temperature for roughly 24 ft of water above the core (i.e. for P = 25 psia or 0.173 MPa) is about 116 C, the ONB point is typically reached at a plate surface temperature of 118 – 125 C depending on the heat flux and flow conditions. Thus, if the maximum clad temperature never exceeds 125 C, there is no possibility of clad or fuel damage in the system. Fuel damage occurs with blister formation, and the blister threshold temperature for both uranium silicide and uranium aluminide fuel is above 500 C,[33] so a maximum clad temperature of 125 C guarantees that fuel damage will not occur.

Thus, for forced flow steady state operation, we need to establish a relationship between power and the pump flow rate at which the onset of nucleate boiling (ONB) point is reached. Similarly, for steady state natural convection operation, we also need to determine the power level where

ONB occurs, where the goal in both cases is to assure that the UMLRR nominal operating point is well within the ONB limits for both forced and free convection operation.

As mentioned above, the NATCON and PLTEMP codes were used to obtain the steady state ONB conditions for the UMLRR. The models are relatively simple, requiring such items as a description of the fuel and channel geometry, the reference pressure and temperature, the radial peaking factor and relative axial power profile, and a set of appropriate hot channel factors. All the calculations used the geometry parameters given in Table 1 on page 3, a radial peaking factor of 2.1, the axial power profile shown in Fig. 4 on page 13, and an LSSS inlet temperature of about 43 C. A full series of cases was run for a 21-element core with UMLRR fuel with and without the hot channel factors shown in Table 11. Several cases were also completed for the WPI fuel but, in all cases, these were not limiting because of the greater number of fuel plates per assembly (18 for the WPI fuel vs. 16 for the UMLRR fuel) -- so there was no need to generate a full data set.

Summary results from the PLTEMP forced flow calculations are shown in Fig. 6, along with an indication of the margin associated with normal operation at 1 MW with a pump flow rate of 1700 gpm. This figure contains curves for both best-estimate "nominal' analysis and with the hot channel factors included to account for uncertainties in the system. The lower curve with the system uncertainties included is considered the upper limit for steady state operation below the ONB point. As apparent, for a nominal flow rate of 1700 gpm, operation at 1 MW gives a margin to ONB of over 2.5.

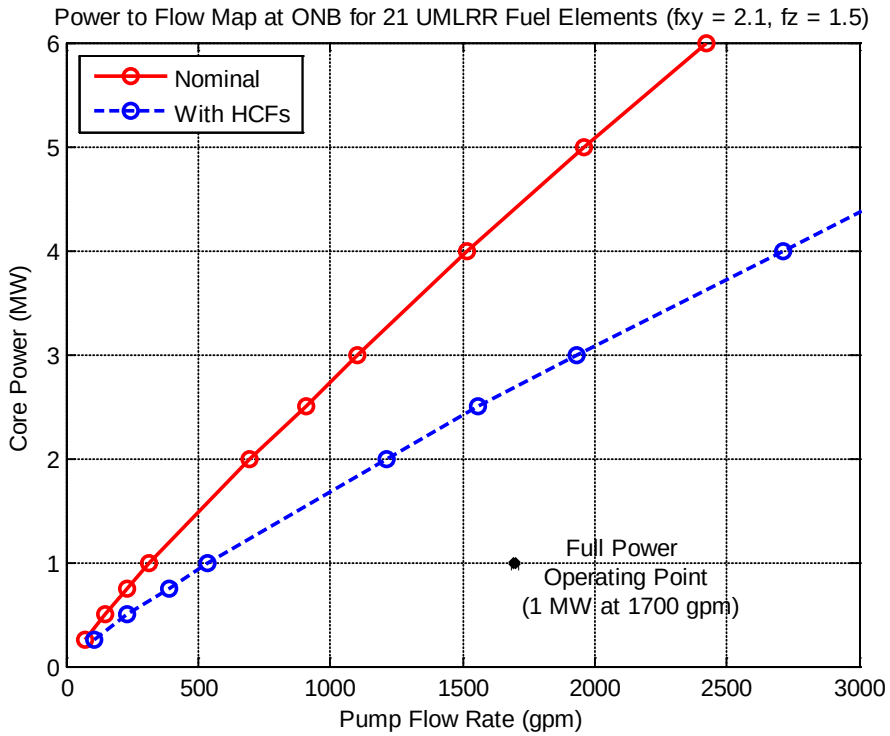

Fig. 6 ONB power to flow map for steady state operation in the UMLRR.

It was noted that the UMLRR fuel was more limiting than the WPI fuel because of the smaller number of fuel plates per assembly. Table 12 demonstrates this behavior quantitatively for a single power level. In particular, it shows the ONB flow rate for a power of 2.5 MW for both the UMLRR and WPI fuel element designs. As seen here, for the case with the engineering hot channels factors HCFs listed in Table 11, for example, the WPI fuel requires a pump flow rate of at least 1312 gpm to stay below the ONB point, whereas the UMLRR element requires about 1561 gpm of flow to prevent localized boiling from occurring. This behavior -- that is, the UMLRR fuel requiring a higher flow rate to stay below ONB -- is similar for all cases (with and without HCFs). Thus, the UMLRR fuel clearly presents a more limiting scenario -- that is why the limiting steady-state ONB power to flow curve shown in Fig. 6 only includes data from the UMLRR fuel cases.

Table 12 ONB flow rate data for P = 2.5 MW for both UMLRR and WPI fuel.

Case Description	UMLRR Fuel	WPI Fuel
nominal best-estimate calculation	909 gpm	744 gpm
with hot channel factors from Table 11	1561 gpm	1312 gpm

Concerning steady-state free convection operation, Table 13 summaries the results from the NATCON ONB runs for the 21-element core models. Here we again see that the UMLRR fuel is more limiting than the WPI design, and that the cases with the hot channel factors (HCFs) are clearly more restrictive. These data suggest that the UMLRR could operate in natural convection mode below the ONB point with a power level as high as 248 kW. This, however, is much larger than the nominal 100 kW operating limit which has been imposed to reduce the production and subsequent escape of radioactive nitrogen from the pool surface. Thus, again, we see that the free flow operating limit of 100 kW gives a margin to ONB of about 2.5.

Table 13 ONB power levels for free flow for both UMLRR and WPI fuel.

Case Description	UMLRR Fuel	WPI Fuel
nominal best-estimate calculation	392 kW	466 kW
with hot channel factors from Table 11	248 kW	313 kW

VII. Operating Limits for Various Transient Scenarios

It should be emphasized that Fig. 6 is only of limited use, since it only sets constraints for operation at steady state -- it does not address the consequences of a transient off-normal condition that is initiated from critical steady state operation. As mentioned previously, there are a series of credible accident scenarios that must be analyzed and, in practice, it is the behavior of these accident sequences that set the real operating limits on the reactor. In most cases, the various initiating events can be classified into either a reactivity-induced or a flow-induced transient and, for the current study, the PARET code is utilized to model and evaluate these situations. In particular, since the limiting criteria for both steady state operation and for credible off-normal protected transients within the UMLRR is the onset of nucleate boiling (ONB) point,

the goal here is to establish a range of operation such that ONB does not occur during a worst-case reactivity or flow transient.

Since a variety of transients can occur, including both rapid and ramp reactivity additions and pump-off and pump-on events, we need to evaluate a full range of possibilities, and then use the most limiting sequence to place actual operating constraints on the UMLRR. In particular, each of the four events (fast reactivity addition, ramp reactivity insertion, loss of flow scenario, and cold water insertion event) are analyzed separately in the following subsections.

VII.1 Rapid Reactivity Addition: Rapid reactivity changes can occur due to the failure of a fixed experiment or other device, due to a rapid cold water insertion event, or possibly due to the rapid ejection of an experimental bayonet from one of the incore radiation baskets. Although never instantaneous in practice, to be conservative, these postulated rapid changes are often modeled as step (or near-step) reactivity changes in the system. In particular, of interest here is the maximum step change in reactivity that can be tolerated under both forced and natural convection flow such that ONB is not exceeded during the transient. Four cases have been selected to evaluate the consequences of this transient, as follows:

Case 1 nominal forced convection:	P_o = 1 MW,	Q = 1700 gpm,	T_{in} = 30 C
Case 2 worst case forced convection:	P_o = 1.25 MW,	Q = 1370 gpm,	T_{in} = 43.3 C
Case 3 nominal free convection:	P_o = 100 k W,	T_{in} = 30 C	
Case 4 worst case free convection:	P_o = 125 kW,	T_{in} = 43.3 C	

For the nominal cases, T_{in} = 30 C was selected arbitrarily in the middle of the range for normal operation (roughly 23 – 35 C). For the worst case runs, the inlet temperature is assumed to be at its LSSS value of 43.3 C (110 F). In addition, for the limiting cases, the initial power level and flow rate are taken at their LSSS values, which coincide with the nominal values as modified by the hot channel factors from Table 11 -- that is, $P = P_{nom} \times 1.25$ and $Q = Q_{nom}/1.24$.

In all the cases, the transient is essentially terminated by an overpower trip signal that is set at 1.25 MW for forced flow and 125 kW for free flow (the LSSS values), with an instrument delay time of 210 msec, an average blade insertion speed of 0.533 m/sec, and the assumption that Blade 4 does not drop with the other safety blades (recall that, from a height of 15 inches withdrawn, Blades 1 – 3 have a combined worth of about 7 dollars as discussed above in Section V.3). In addition, all the runs use a radial peaking factor of 2.1 and the axial profile shown in Fig, 4 with f_z = 1.50. To find the maximum reactivity allowed in the PARET runs, the step reactivity addition was increased in units of 0.01 $\%\Delta k/k$ = 0.1 mk until ONB is reached at some point in the transient. The highest value of step reactivity used that did not result in hitting the ONB limit was then tabulated as the desired ρ_{max}.

Table 14 summarizes the results of these four step reactivity cases. As apparent, the range of step changes that can be tolerated varies from about 6.4 mk to 8.6 mk, depending on the specific assumptions that are made. Clearly, the forced flow case with LSSS values for P_o and Q gives the most restrictive situation, and the two natural convection simulations are least restrictive, indicating that an 8.4 mk step change (about 1.1$) will not lead to ONB before the reactor protective system begins to shut down the transient. For the limiting case (i.e. Case 2), the PARET calculations indicate that a 6.4 mk reactivity addition does not lead to ONB during the transient, but that a 6.5 mk step change exceeds the ONB safety limit for a short time period.

Table 14 Maximum step reactivity insertion allowed without hitting the ONB limit.

Case #	Max reactivity insertion	P_{max} (MW)	Max T_{clad} (^oC)
1 -- nominal forced flow	7.2 mk	9.78	124.5
2 -- worst case forced flow	6.4 mk	6.60	121.1
3 -- nominal free flow	8.6 mk	13.5	121.2
4 -- worst case free flow	8.4 mk	10.6	120.6

The current UMLRR Technical Specifications[34] limit the worth of a single experiment to 0.5 %Δk/k = 5 mk. Since failure of an experiment is the most likely initiating event for a rapid reactivity insertion transient, the above calculations suggest that the maximum single experiment worth specification should remain unchanged -- since a 5 mk step change is well within the upper limit of 6.4 mk. To see this, a step change of 5 mk was made with the conditions as noted above for Case 2. The resultant power vs. time and the maximum coolant, clad, and fuel temperatures vs. time for the transient are shown for this case in Fig. 7. As apparent, although the power reaches a peak of about 3.5 MW, the high power interval is very short with only a moderate amount of energy being deposited. The power starts to decrease immediately as the blades start to enter the core shortly after 0.21 seconds into the transient (note that this happens just after the 210 msec instrument delay time used as part of the PARET model). The clad and fuel temperatures peak shortly after the power peak, and then these also drop rather rapidly, with the transient being essentially over within 1 second of the initial step change. Since the initial flow rate is maintained, the decay heat is easily removed and all the temperatures eventually decrease until they approach equilibrium with the inlet temperature. Clearly, with a maximum clad temperature of about 95 C, there is a large margin to ONB throughout the transient -- thus, even the very conservative ONB safety limit is not exceeded in the event of a worst-case experiment failure with a reactivity worth of 5 mk.

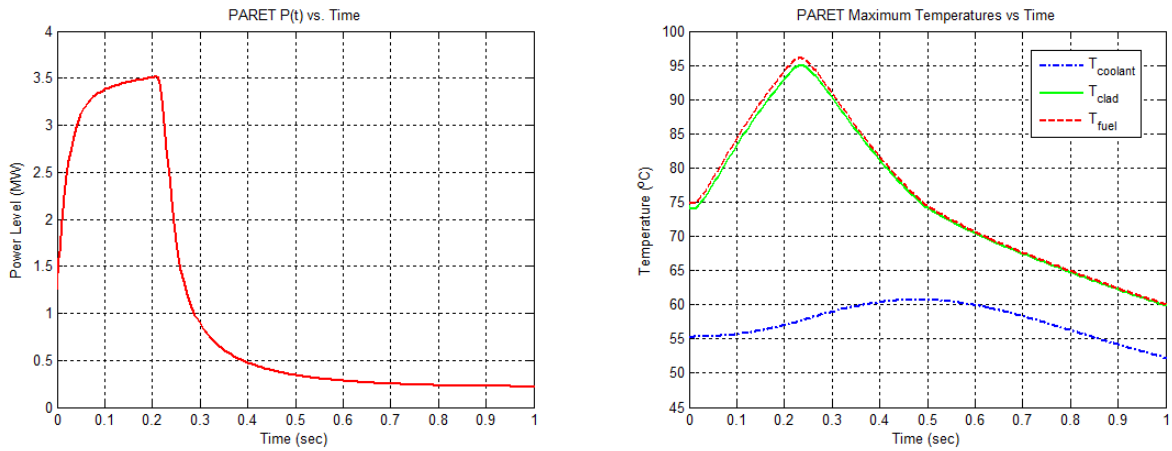

Fig. 7 Response to 5 mk step change with LSSS values of P_o, Q, and T_{in} with UMLRR fuel.

As a final PARET run for the step reactivity cases, the same 5 mk step-change scenario as above was simulated using the WPI fuel specifications instead of the UMLRR fuel data. For the steady state cases, the UMLRR fuel has already been shown to be more limiting than the WPI fuel because of the fewer number of fuel plates per assembly. This same behavior is expected here, but the simulation was run for completeness and to quantify the additional margin to ONB that can be expected with use of the WPI UAl_x-Al fuel elements. The results of this simulation are shown in Fig. 8, where we see the same basic dynamic behavior as apparent in Fig.7, but here the peak temperatures are all lower than for the simulation with UMLRR fuel. In particular, the peak clad temperature in the WPI fuel for a 5 mk step change in reactivity is only about 86 C, which is roughly 9 C less than for the UMLRR fuel. Thus, as expected, the UMLRR fuel design clearly presents the more limiting situation -- and no further UMLRR vs. WPI fuel comparisons are needed or warranted.

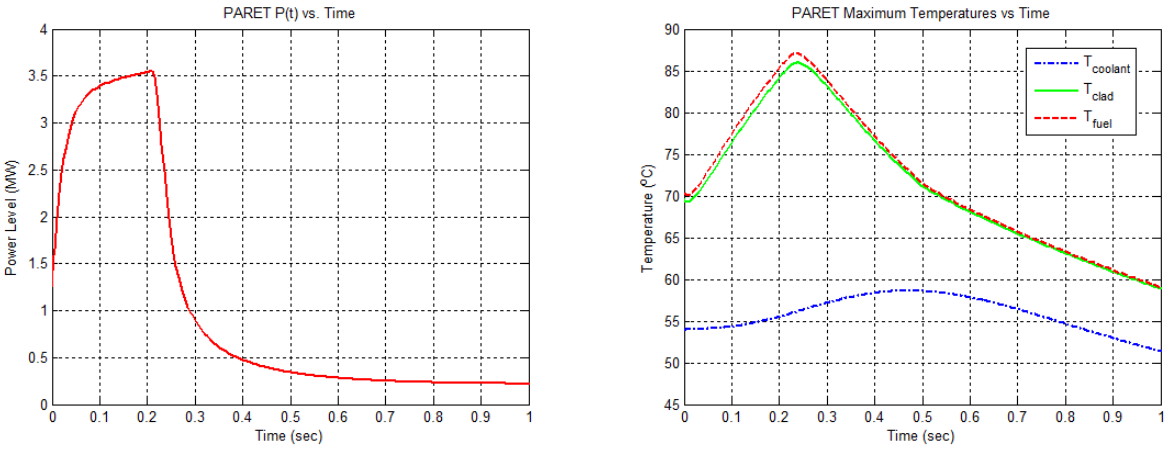

Fig. 8 Response to 5 mk step change with LSSS values of P_o, Q, and T_{in} with WPI fuel.

VII.2 Ramp Reactivity Insertion: The inadvertent withdrawal of a control blade is the most obvious initiating event that could be associated with a postulated ramp reactivity insertion. As a check on the actual blade movement rates, the blade speeds and maximum differential worths were measured as part of the annual UMLRR blade calibrations performed in Jan. 2015. The safety blades' insertion rate was about 4 inches/min and the maximum differential worth of Blade 4 was a little under 0.3 %Δk/k per inch, which gives a maximum insertion rate of about 0.02 %Δk/k per second -- which is lower than the Technical Specification (TS) limit of 0.025 %Δk/k per second.[34] For the RegBlade, the insertion rate was about 55 inches/min and the maximum differential worth was under 0.025 %Δk/k per inch. These values combine to give a reactivity insertion rate of 0.023 %Δk/k per second -- and, as for the safety blades, this is well below the TS limit of 0.054 %Δk/k per second for the RegBlade.[34]

As a conservative evaluation, the analysis here focuses on a ramp insertion speed of 0.07 %Δk/k per second = 0.7 mk/s, with simulations performed for both forced and natural convection operation. Other cases were run with lower ramp speeds, but the results were very similar except for the timing of the over-power trip, so they will not be described here. Since the goal is to identify the worst-case consequences of an inadvertent blade withdrawal, the 0.7 mk/s ramp insertion simulations in PARET assumed a range of values for initial power, inlet temperature, and pump flow rate.

For specificity, the six cases discussed below are identified as follows:

Case 1 forced flow with a 0.7 mk/s reactivity insertion rate with P_o = 1.00 MW, T_{in} = 43.3 C, and Q = 1370 gpm

Case 2 same as Case 1 with P = 1.25 MW

Case 3 same as Case 1 with T_{in} = 30.0 C and Q = 1700 gpm

Case 4 natural convection flow with a 0.7 mk/s reactivity insertion rate with P_o = 100 kW and T_{in} = 43.3 C

Case 5 same as Case 4 with P ≈ 125 kW

Case 6 same as Case 4 with T_{in} = 30.0 C

Note that the remaining simulation parameters, such as the delay time, safety blade insertion rate upon scram, blade worth profile, etc., were the same as used above in the step insertion cases -- in fact, these parameters were held fixed for all the PARET runs. For the power trip point, 1.25 MW was used for the forced flow cases and 125 kW was used for all the natural convection runs.

The key results for the ramp reactivity insertion cases are summarized in Figs. 9 and 10 for the forced flow and natural convection cases, respectively. Clearly Cases 1-3 focus on forced flow mode and Cases 4-6 highlight the natural convection mode. The 2nd case in each set simulates the reactor operating approximately at its LSSS point just before the ramp insertion occurs. However, as seen in the middle plots in Figs. 9 and 10, the power setpoint is reached nearly instantaneous, and the blades start to drop shortly afterwards (after the instrument delay) -- and the temperature change over this short an interval is negligible. To observe the power rise and temperature increase during the ramp reactivity insertion, the 1st case in each set has the initial power at its nominal maximum value for the given operational mode, which then increases due to the reactivity insertion until the overpower setpoint is reached and the blades start to drop. For these cases, a small rise in the maximum system temperatures is seen over the interval for the power rise.

Finally, the 3rd set of forced and natural convection runs, as seen in the bottom set of plots in Figs. 9 and 10, represent nominal expected behavior during routine operation of the reactor, with the use of nominal P_o, T_{in}, and pump flow rates for the two operating modes. The behavior of these cases looks very similar to the top plots, except that the base temperatures are lower because of the lower inlet temperature and the larger coolant flow rate for the forced flow case.

As a last point, we note that the time interval for each of the transients is only 3 seconds. However, for the natural convection cases shown in Fig. 10, the time scale goes from 57 to 60 seconds. For these cases, the first 57 seconds of simulation time were used to get the natural convection flows in both the average and hot channels to converge, and then the ramp reactivity insertion was initiated from equilibrium at t = 57 seconds.

Well, to summarize the ramp reactivity insertion cases, it is safe to say that these accident scenarios represent relatively mild transients to the overall system. In all cases, the reactor protection system is assumed to work and, with an instrument delay time of only 0.21 seconds, there is not much time for the reactor power and system temperatures to increase significantly. Accordingly, there is no real possibility of reaching the UMLRR onset of nucleate boiling (ONB) safety limit for this class of transients. Thus, a protected ramp reactivity insertion is not a limiting transient scenario within the UMLRR!

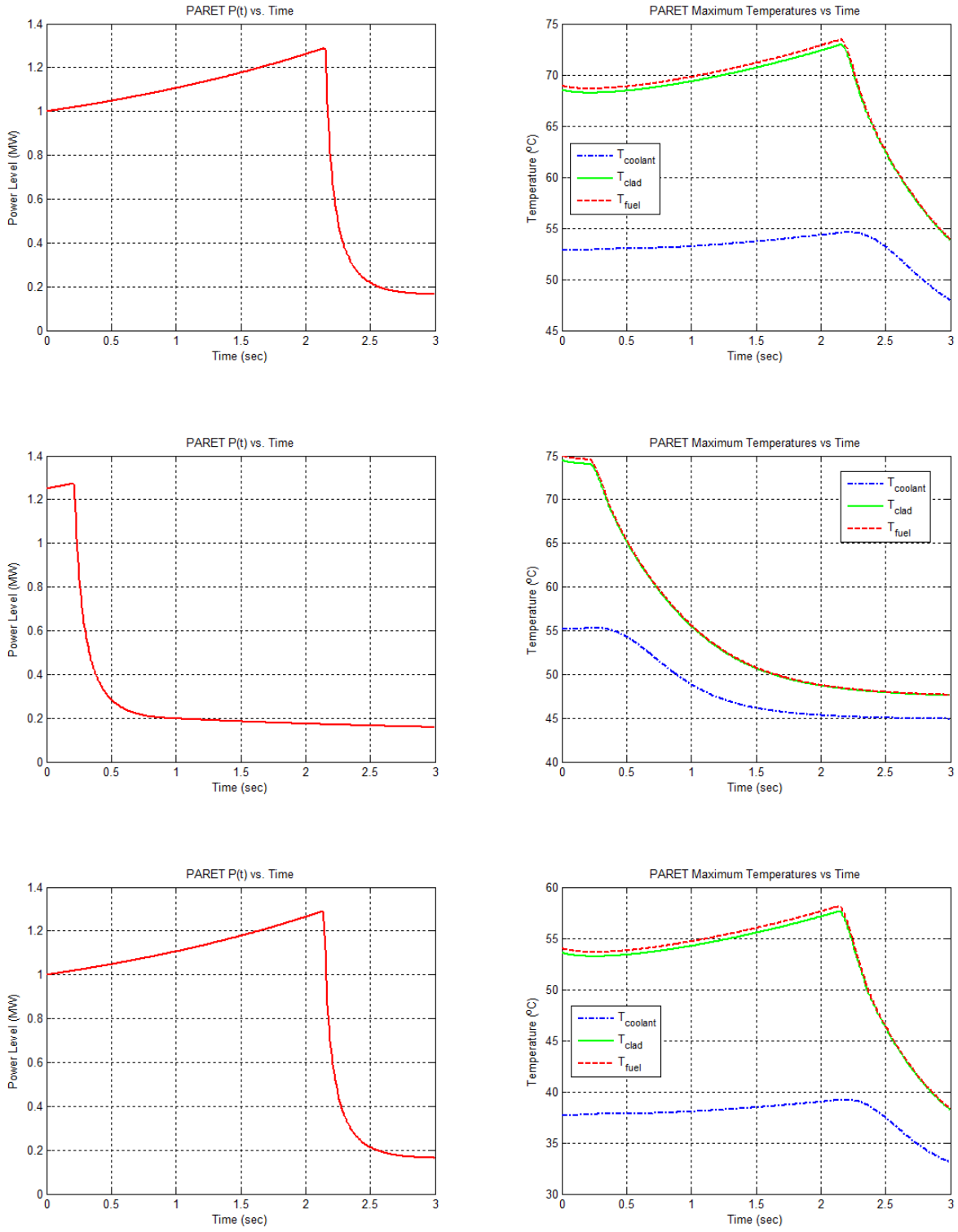

Fig. 9 Response to 0.7 mk/s ramp in forced flow mode with various initial conditions.

Top Plots: Case 1 -- forced flow with P_o = 1.00 MW, T_{in} = 43.3 C, and Q = 1370 gpm
Middle Plots: Case 2 -- forced flow with P_o = 1.25 MW, T_{in} = 43.3 C, and Q = 1370 gpm
Bottom Plots: Case 3 -- forced flow with P_o = 1.00 MW, T_{in} = 30.0 C, and Q = 1700 gpm

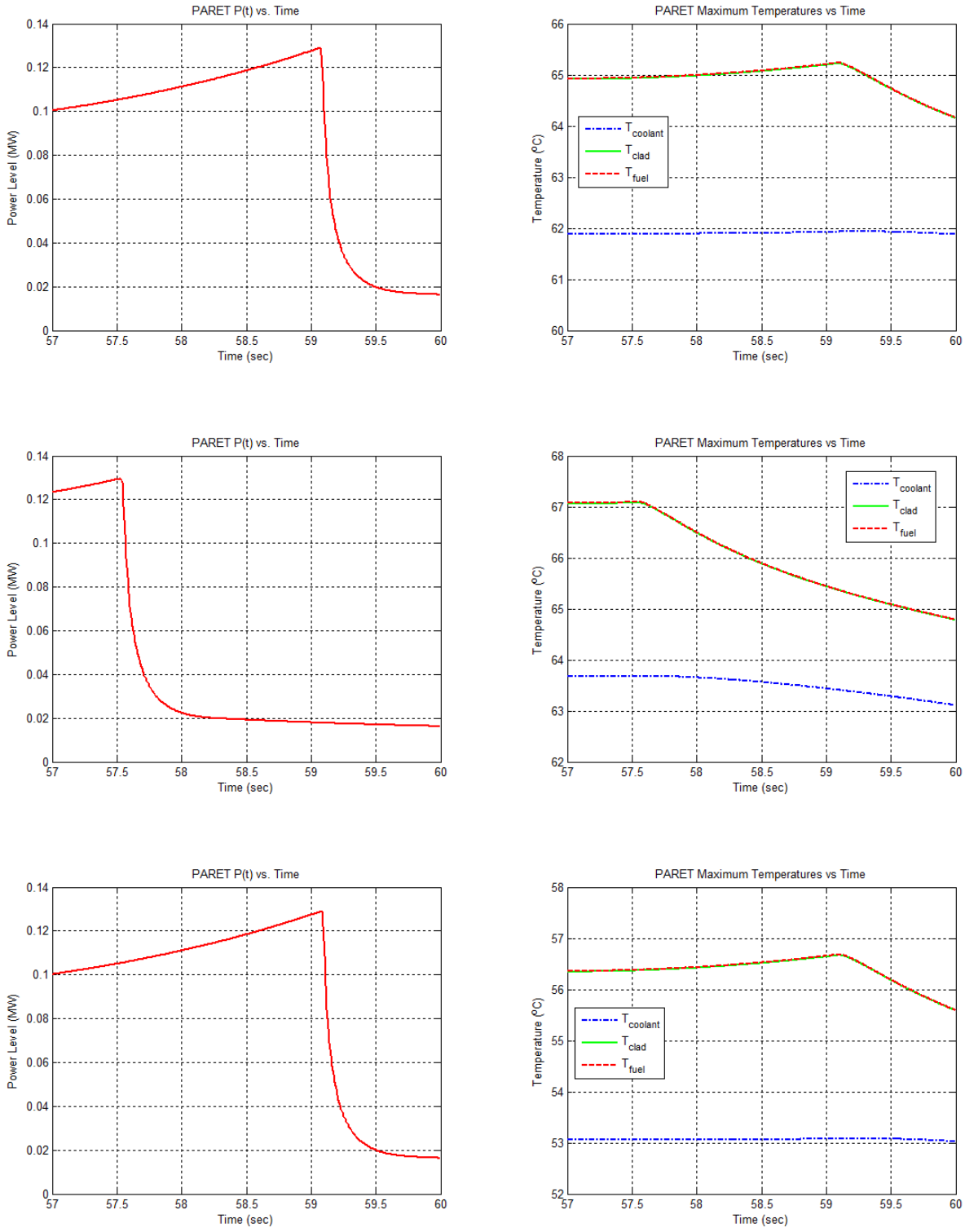

Fig. 10 Response to 0.7 mk/s ramp in free flow mode with various initial conditions.

Top Plots: Case 4 -- natural convection flow with P_o = 100 kW and T_{in} = 43.3 C
Middle Plots: Case 5 -- natural convection flow with P_o = 125 kW and T_{in} = 43.3 C
Bottom Plots: Case 6 -- natural convection flow with P_o = 100 kW and T_{in} = 30.0 C

VII.3 Loss of Pump Flow: During forced down-flow operation, the primary pump supports a nominal flow rate of about 1700 gpm. As discussed in Section V.5, a minimum of about 68% of this total flow goes through the fuel elements to remove the energy deposited via fission and radioactive decay. If, for any reason, forced flow is lost, then the downward flow ceases and upward flow is initiated by the difference in fluid density in the heated channels and the surrounding pool, which eventually reaches equilibrium natural convection flow when the buoyancy forces balance the fluid friction forces in the coolant channels. A loss of flow scenario would occur with a pump failure or a loss of electrical power event. These are credible initiating events so the consequences following a loss of flow accident must be evaluated to guarantee that no safety limits are exceeded.

As discussed in Section V.4 and shown in Fig. 5, the flow rate following a sudden pump-off event behaves much like a decaying exponential profile, with the flow rate going to essentially zero in about 10 seconds. This flow profile was input into PARET to drive all the loss of flow (LOF) models. Three cases, involving different combinations of P_o, T_{in}, and Q_o, were analyzed as follows:

Case 1 LOF scenario with P_o = 1.25 MW, T_{in} = 43.3 C, and Q_o = 1700 gpm

Case 2 same as Case 1 with Q_o = 1370 gpm

Case 3 LOF scenario with the reactor initially at nominal conditions (P_o = 1.00 MW, T_{in} = 30.0 C, and Q_o = 1700 gpm)

The summary results from these three LOF simulations are presented in Fig. 11. As apparent, all three cases behave in a similar manner, with some specific differences that are related to the different operating states and/or initial conditions. For example, with a scram setpoint of 1370 gpm for all cases, Case 2 scrams nearly instantaneous (i.e. after the short instrument delay) because the reactor is assumed to be operating at the low-flow setpoint prior to pump failure. In Cases 1 and 3, however, the trip occurs after about 1.5 seconds into the transient since, according to Fig. 5, the core flow rate drops to about 80% of initial capacity in about 1.5 seconds after the pump-off events starts. Similarly, the peak initial temperatures occur for Case 2, since this scenario has the highest power and lowest rate flow rate combination of the three cases shown here.

Concerning the temperature profiles vs. time, these are more easily explained with the help of some addition information -- specifically, a mass flux vs. time curve. In particular, global and focused views of the mass flux vs. time profile are given for Case 1 in Fig. 12. This set of curves is similar for all cases, but Case 1 was selected since it represents the most practical worst-case scenario for a LOF event where, initially, the pump flow rate is at nominal conditions (1700 gpm), but the power level and inlet temperature are at their LSSS values. With pump coast down beginning at t = 0 (with a negative mass flux because the flow is down through the core), the flow rate decreases in a near-exponential fashion towards zero in about 10 seconds, and then natural convection begins, first in the hottest channel and then in all the other heated channels, with flow upward through the core. After the initial brief temperature rise due to a decreasing flow rate, and then the rapid drop due to the insertion of the blades and resultant rapid decrease in power, the core temperatures then start to increase as the flow rate decreases to zero and actually changes sign as upflow begins. At this time, there is a strong interrelationship between temperature and flow rate, since in natural convection flow, the coolant temperature and density changes are what initiates the buoyancy-driven flow, yet the coolant flow is what removes the

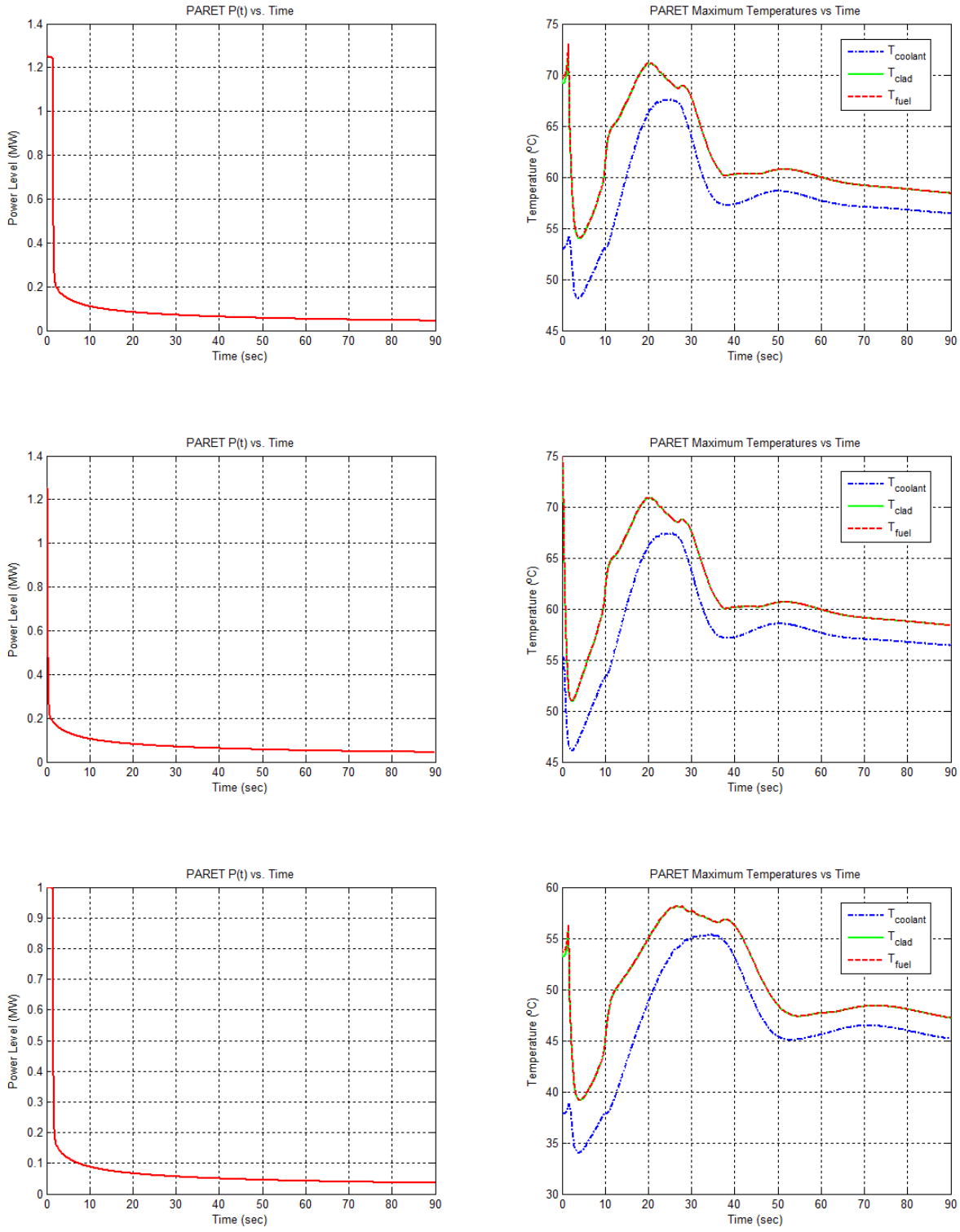

Fig. 11 Behavior of loss of flow (LOF) transient from various operating conditions.

Top Plots: Case 1 -- LOF scenario with P_o = 1.25 MW, T_{in} = 43.3 C, and Q_o = 1700 gpm
Middle Plots: Case 2 -- LOF scenario with P_o = 1.25 MW, T_{in} = 43.3 C, and Q_o = 1370 gpm
Bottom Plots: Case 3 -- LOF scenario with P_o = 1.00 MW, T_{in} = 30.0 C, and Q_o = 1700 gpm

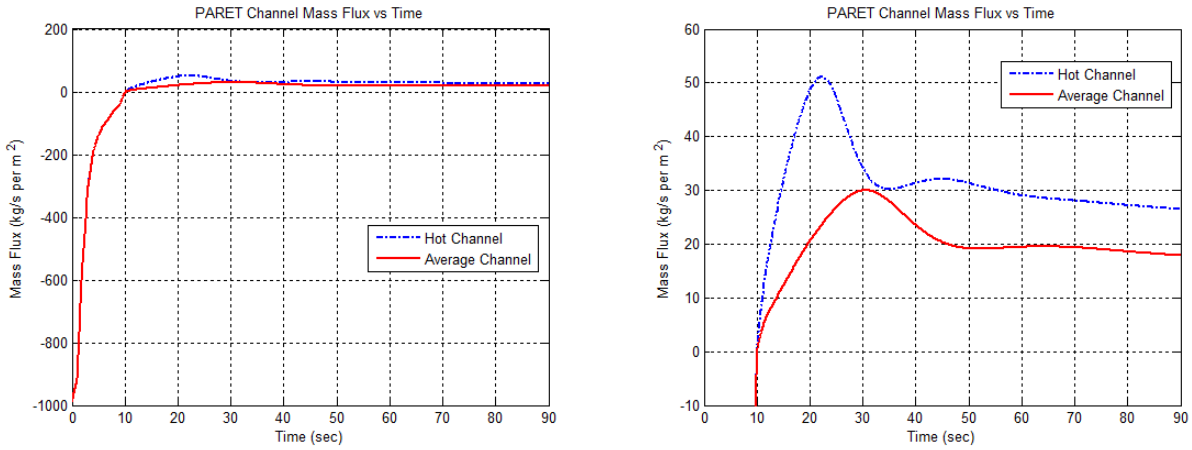

Fig. 12 Mass flux versus time for the Case 1 LOF simulation
(left plot: global view, right plot: focused view after flow inversion).

energy from the fuel plates -- and this strong interdependence is seen in the temperature and flow rate profiles after about 10 seconds in Figs. 11 and 12, respectively. Eventually the system temperatures and individual channel flow rates stabilize and then continue to decrease slowly as the internal heat source (i.e. decay heat) steadily decreases in time.

Although the flow reversal phenomena following a LOF event in the UMLRR is quite interesting in itself, the most important aspect of the above simulations from the reactor safety perspective is the relatively low temperatures that were observed. In all cases, the highest clad temperature was under 75 C, which clearly gives a significant margin to the ONB safety limit. Thus, as observed for a ramp reactivity insertion event, there is also no real possibility of reaching the onset of nucleate boiling (ONB) safety limit for a protected loss of flow (LOF) transient within the UMLRR. Accordingly, a protected LOF event is another non-limiting transient scenario within the UMLRR!

VII.4 Cold Water Insertion Event: Positive reactivity can be inserted into the reactor core in a number of ways, including withdrawal of control, failure of an experiment, etc., or by the sudden insertion of cold water into the core. This latter scenario, which is referred to as a "cold water insertion event," is related to a combination of negative reactivity feedback and a rapid decrease in core temperature. As shown in Table 6 on page 15, the total isothermal temperature coefficient in the UMLRR is about -1.43e-4 $\Delta k/k/^{o}C$, so a rapid decrease in temperature would indeed lead to an increase in reactivity. And, a prompt decrease in temperature is mostly likely to result from either of two operator actions:

1. Turning on the secondary cooling system during forced flow operation on a cold winter day when the sump temperature is low.
2. Turning on the primary pump during natural convection operation.

To address the first scenario, we first note that it has already been established in Section VII.1 that the core transient associated with a 5 mk step change in reactivity does not exceed the UMLRR ONB safety limit (actually it has a greater than 20 ^{o}C safety margin to ONB). Thus, using 5 mk as an upper limit and a conservative 25% safety factor on the value of the isothermal

temperature coefficient, α_{ITC}, the maximum temperature change allowed can be determined as follows:

$$\Delta\rho = \alpha_{ITC}\,\Delta T$$

or

$$\Delta T_{max} = \frac{\Delta\rho_{max}}{\alpha_{ITC_{max}}} = \frac{5\times10^{-3}\ \Delta k/k}{1.25\times(-1.43\times10^{-4}\ \Delta k/k\ \text{per}\ ^{o}C)} \approx -28\ ^{o}C$$

Thus, to achieve a 5 mk positive reactivity step insertion, the core coolant temperature would have to decrease nearly instantaneously by about 28 ^{o}C -- and, for several reasons, this is simply not possible by turning on the secondary cooling system!

First, with the current flow arrangement in the UMLRR, the primary flow enters the pool on the bulk pool side, mixes with the roughly 76000 gallons of water in the pool, and then enters the core channels via suction flow from the top to the bottom of the fuel. A sudden decrease in the pool inlet temperature at a 1700 gpm flow rate gets delayed by several minutes, and the warmer inlet water is mixed with the existing pool water before it reaches the core inlet. Thus, a sudden decrease in core inlet temperature due to a change in pool inlet temperature is not possible with the current cross-pool flow scheme.

If the flow arrangement was ever changed to have a straight connection with the core inlet coming directly from the outlet of the heat exchanger, the magnitude of the temperature changes and the delay times involved still would prohibit any sudden large change in core inlet temperature from occurring. To see this, some data from a recent energy balance experiment are shown in Fig. 13 -- please note that the temperature scale here is in ^{o}F as recorded by the reactor instrumentation system, whereas most of the other temperature references in this report are in ^{o}C. The goal of the experiment was to look at different cooling levels -- with no cooling initially and maximum cooling at the end, with the reactor at full power during the entire experiment.

Of most interest here, however, is the behavior observed at t = 1.5 hours into the experiment when the secondary pump is turned on, and again at about t = 2.8 hours when the cooling fans in the cooling tower are turned on. Roughly, the ΔT seen in the sump water due to these operator actions is about 25-30 ^{o}F, and on the secondary side of the heat exchanger it is about 20-25 ^{o}F. However, the temperature variation on the primary side of the heat exchanger and in the pool inlet temperature is less than 10 ^{o}F. In addition, although the temperature transients appear to be very rapid in the figures shown, the time scale here spans 4.5 hours -- so this is a little misleading. In particular, with focus at t = 1.5 hours, the 8 ^{o}F change in pool inlet temperature takes place over an 80-second interval. Thus, as stated above, a large sudden decrease in core inlet temperature is simply not possible by turning on the secondary cooling system!

The second possible scenario for rapidly changing the core temperatures involves the primary pump being activated with the reactor initially at nominal high power conditions (i.e. 100 kW) in natural convection mode. In this flow mode, the flow rate is up through the core at only 1-2 cm/s. At this flow rate, even relatively low power levels can produce a significant temperature rise in the core. Then, if the pump is turned on, the warm water in the core is rapidly replaced with the cooler pool water from above the core, leading to the so-called “cold water insertion event.” Thus, with negative feedback and a rapid decrease in core temperature, the pump-on event rapidly inserts positive reactivity into the system, with a subsequent rise in power over

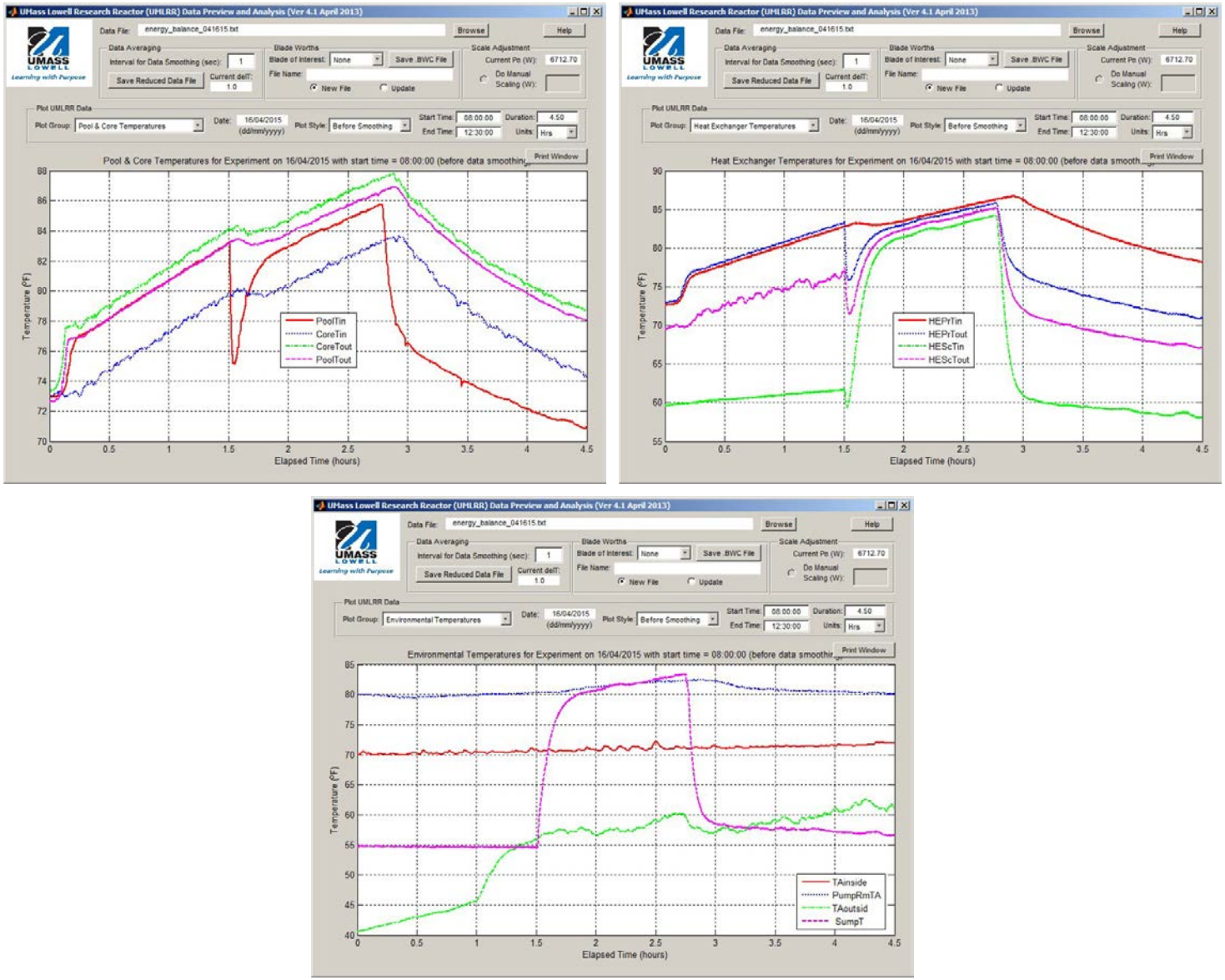

Fig. 13 Typical temperature transients associated with the secondary side cooling system.

time. However, unlike the transient caused by a change on the secondary side, the pump-on transient on the primary side is relatively fast since the pump speed approaches full capacity in only a few seconds.

A PARET model was constructed to analyze this pump-on event. As in the other transient scenarios, three different cases were studied to represent various initial operating conditions, as follows:

Case 1 pump-on scenario with P_o = 100 kW and T_{in} = 43.3 C

Case 2 same as Case 1 with P_o = 125 kW

Case 3 pump-on scenario with the reactor initially at nominal free-flow conditions (P_o = 100 kW and T_{in} = 30.0 C)

The summary results from these three pump-on simulations are given in Fig. 14. All three cases behave similarly, with the increasing flow rate causing a decrease in the system temperatures, with a subsequent positive reactivity increase and corresponding increase in power. Then, once the power setpoint is hit, the blades drop and the power and temperatures drop accordingly. However, although very similar, there are some unique details that are directly related to the various initial states selected for a specific case. For instance, with a scram setpoint of 125 kW for all cases, Case 2 scrams nearly instantaneous (i.e. after the 0.21 seconds associated with the instrument delay time that is input to PARET) because the reactor is assumed to be operating at its LSSS setpoint for natural convection prior to turning on the pump. In Cases 1 and 3, however, the trip occurs after about 1.8-1.9 seconds into the transient since it simply takes a little longer in these cases for P(t) to increase to the power setpoint. Similarly, the peak initial temperatures occur for Case 2, since this scenario has the highest power and inlet temperature combination of the three cases shown here. Finally, it should be noted that all the initial peak temperatures are a little higher than expected because the PARET model only allows the specification of a single initial flow rate. Since the core average value was used here -- which is a little lower than expected in the hot channel -- this assumption leads to slightly higher peak initial temperatures.

From a reactor safety perspective, the pump-on event leads to a relatively low-risk scenario that is much less severe than a step reactivity insertion. In all cases, the highest clad temperatures were associated with those seen at the initiation of the event. Following the cold water insertion associated with the pump being activated, P(t) does increase for a short time until the reactor scrams, but during this time the temperatures are still decreasing because of the increased forced flow cooling that has been introduced. Thus, the conclusion here is that a protected pump-on event from steady state natural convection operation is certainly not a limiting transient scenario for the UMLRR!

VII.5 Operating Limits Summary: The purpose of Section VII of the current report was to study the consequences associated with different reactivity-induced and flow-induced transients within the UMLRR, and to use these accident scenarios to set proper limits for safe operation of the facility under all credible event scenarios. In all cases, it was assumed that the reactor protection system works as designed, and that three of the safety blades drop into the core after an appropriate delay time following either a high-power or low-flow trip signal. Of the off-normal conditions addressed here, only the near instantaneous insertion of reactivity scenario lead to clad temperatures that, with sufficient positive reactivity addition, could exceed the ONB

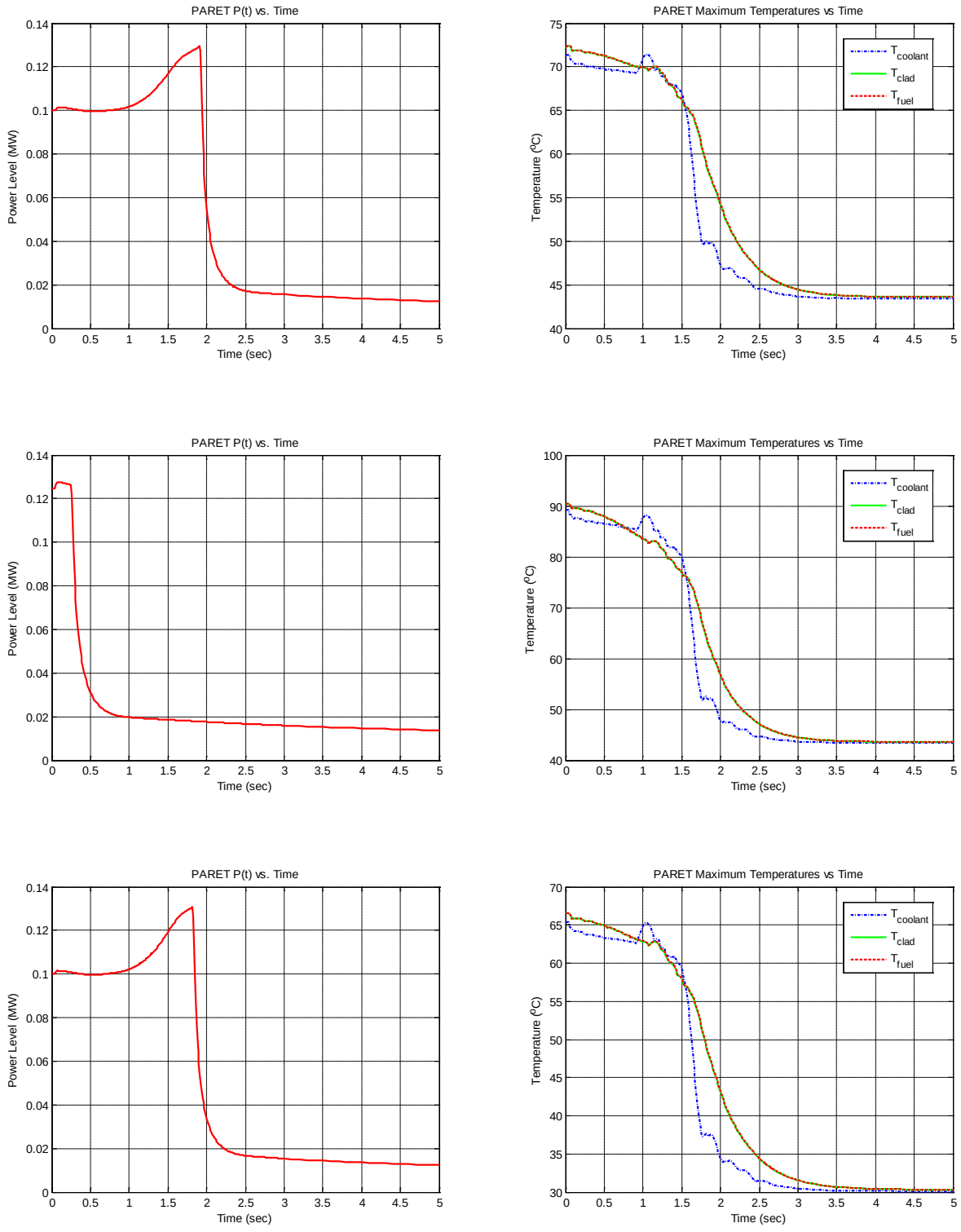

Fig. 14 Behavior for a pump-on event from various operating conditions.

Top Plots: Case 1 -- pump-on scenario with P_o = 100 kW and T_{in} = 43.3 C
Middle Plots: Case 2 -- pump-on scenario with P_o = 125 kW and T_{in} = 43.3 C
Bottom Plots: Case 3 -- pump-on scenario with P_o = 100 kW and T_{in} = 30.0 C

safety limit. Because of this behavior, a series of PARET simulations were made to identify the maximum step reactivity addition that could be allowed such that the ONB safety limit would not be reached during the transient. This sensitivity study is summarized in Table 14 on page 28, with the conclusion that, for the worst-case scenario of the reactor operating at its forced flow LSSS point of P = 1.25 MW, T_{in} = 43.3 C, and Q_{pump} = 1370 gpm, the maximum step reactivity that can be allowed is 6.4 mk = 0.64 %Δk/k. This sets the upper reactivity limit for any fixed experiment or other device in the reactor that could possibly fail in a catastrophic manner that gives rise to a rapid increase in positive reactivity. However, since the current Technical Specifications[34] limit the maximum worth of a single experiment to 0.50 %Δk/k, there already is a comfortable built-in safety factor between the maximum allowed reactivity addition identified here and the existing limit set by administrative procedure. Thus, no change should be required in this particular TS requirement.

VIII. New Technical Specification Considerations

The safety analysis for a given reactor serves as the basis for the formal Technical Specifications (TS) for the facility. The purpose of the Technical Specifications is to explicitly "state the operating limits and conditions and other requirements for the facility to acceptably ensure protection of the health and safety of the public."[1] The last formal safety analysis[26] for the UMLRR was performed as part of the conversion from HEU to LEU fuel,[9-10] and the current Technical Specifications[34] refer explicitly to Ref. 26 to justify the operating limits for the UMLRR. The purpose of this section of the current document is to identify where and how the updated safety analysis performed during the summer of 2015 will affect the TS for the UMLRR going forward.

First, it should be emphasized that the basic safety criteria and philosophy for safe operation of the UMLRR remains unchanged. The reactor at UMass-Lowell has been operating safely for nearly 40 years, and throughout that time, the very conservative safety limit criteria for both steady state operation and for credible off-normal protected transients has been the onset of nucleate boiling (ONB) condition. Since the ONB point is typically reached at a clad surface temperature of 118 – 125 ^{o}C depending on the heat flux and flow conditions, setting the upper safety limit for steady state operation and for credible off-normal situations at the ONB point guarantees that fuel damage will not occur. Although very conservative, this safety limit has not adversely constrained facility operations for the last 40 years, so there is no good reason to abandon this conservative safety limit for future operations.

However, there has been a change in how this ONB safety limit is applied in the current safety analysis relative to the previous analyses.[26] In particular, Ref. 26 uses the steady-state ONB power to flow map to establish formal operational limits for the UMLRR. This curve (see Fig. 3.2 in Ref. 26 and/or Fig. 6 in this document) establishes a relationship between the steady state power level and the pump flow rate at which the onset of nucleate boiling (ONB) point is reached. The previous safety analysis[26] rigorously applied this operational curve -- that was derived from steady state data -- to both steady state and transient operation of the facility. However, as seen in the many transient P(t) profiles in the current document, the higher power levels seen during an off-normal event often occur over very short time intervals, which limits the energy deposition and the increase in the system temperatures that are observed. Thus, applying a steady state power vs. flow relationship to a power peak that lasts only a fraction of a second is simply too conservative and overly restrictive. Accordingly, for the current safety

analysis, the steady state power to flow map is only used to show that the nominal UMLRR operating point is well below the ONB steady state safety limit. In particular, to emphasize this point, we further note that the steady state ONB power to flow map was not used in any capacity to address the transient situations. Instead, each type of credible accident scenario was analyzed separately and it has been shown that ONB conditions are not expected for any protected event except for a step reactivity insertion worth over 6.4 mk.

The best example that emphasizes how this change in analysis philosophy affects the Technical Specifications relates to the loss of flow (LOF) transient. In Refs. 26 and 34 there is a lot of discussion concerning this event and how it is used to set the forced convection LSSS conditions for the UMLRR, based primarily on the steady state ONB power to flow map and the pump coast down curve (Figs. 3.2 and 3.7, respectively, in Ref. 26). However, as shown in Section VII.3 in the current report, the LOF event is a non-limiting accident scenario, with relatively small temperature increases in the early part of the transient, with rapidly decreasing power and temperature profiles after the control blades drop, and with relatively low and slowing varying temperatures after flow reversal and the development of natural convection flow. At no point in the transient does the system even come close to the ONB point -- in fact, in the "worst-case" LOF scenarios addressed here, the peak temperatures in the system occur at steady state operation prior to initiation of the LOF event. Thus, this accident scenario should not be used to set operational conditions for the UMLRR!

As another example that emphasizes how overly conservative (and restrictive) the steady state ONB power to flow curve can be, consider the step insertion of 5 mk of reactivity into the core. For worst-case conditions for prior operation (i.e. with P_o = 1.25 MW, Q = 1370 gpm, and T_{in} = 43.3 C), Fig. 7 on page 28 shows that the peak power prior to the blades dropping into the core reaches about 3.5 MW, but that, even for this high power level, the peak clad temperature is only about 95 ^oC. This transient power-temperature relationship exists because of the relatively short duration of the higher power levels.

However, based on the steady state ONB power to flow curve with the HCFs included as shown in Fig. 6 on page 25, at a flow rate of 1370 gpm, the maximum steady state power allowed to avoid ONB is slightly over 2 MW. Thus, if this curve was used to limit operations, then the 5 mk step change with its observed 3.5 MW peak at about 0.2 seconds into the transient would not be allowed. Clearly, this is overly restrictive since the maximum transient clad temperature observed was only about 95 ^oC -- which gives more than a 20 ^oC safety margin to the ONB point.

Well, based on the above arguments and examples, in this work, the steady state ONB power to flow map is used for nothing other than to show that the nominal steady state operating point in the UMLRR (i.e. where P_o = 1 MW, Q = 1700 gpm, and a mid-range value of T_{in} = 30 C) is well within the acceptable operating region (as shown explicitly in Fig. 6). For the transient analyses, staying below the ONB point during the transient is the established requirement, and Section VII in this report shows that, using conservative assumptions, this is achieved for all the transients analyzed, except for a step reactivity insertion of greater than 6.4 mk. Thus, the limiting accident scenario for the UMLRR is a step insertion of greater than 6.4 mk!

Based on the detailed results of the current safety analysis and the change in analysis philosophy as discussed above, a number of changes will be needed to the Technical Specifications (TS) for

the UMLRR. In particular, referring specifically to the notation and section numbers used in Ref. 34, the following general modifications are recommended:

1. In Section 2.1.1 concerning the Safety Limits in forced convection flow, Specification 1 should not refer explicitly to the steady state ONB power to flow map -- in fact, this figure probably should be removed from the TS altogether. Instead, the safety limit should refer to ONB as the upper limit for operation during both steady state and transient operation.

   Another approach, of course, would be to include the steady state ONB power to flow map (i.e. Fig. 6 on page 25) as part of the TS, but then to clearly restrict the specification to apply to only steady state operation.

2. In Section 2.1.2 concerning the Safety Limits for natural convection flow, the value of the maximum thermal power should be changed from 0.335 MW to 0.248 MW. This decrease in power is due primarily to the increased radial and axial peaking factors used in this analysis (f_{xy} = 2.1 and f_z = 1.5 for the current analysis, whereas f_{xy} = 1.45 and f_z = 1.39 were used in the previous safety study as discussed in Refs. 25 and 26, respectively). Also, it should be emphasized that this power value is a steady state limit.

   An alternate approach is to write the specification to focus on the ONB point during both steady state and transient operation during natural convection operation and not specifically mention a maximum steady state value. The nominal natural convection power level is set at 100 kW because of N-16 considerations, and really has nothing to do with the 248 kW steady state ONB point. In fact, this value is not really meaningful other than for steady state operation -- which is similar to the steady state ONB power to flow map as discussed above for forced flow operation.

3. In Section 2.2.1 concerning the limiting safety settings (LSSS) for forced flow, the LSSS value for the flow rate, W, should be changed to W = 1370 gpm.

   In general, the Limiting Safety System Settings (LSSS) represent the values of the power, flow rate, inlet temperature, and pool water height which, if violated, result in automatic control action. These are set to prevent the Safety Limits from being exceeded. In the current work, with focus on the ONB safety limit during both steady state and transient operation, the LSSS values for power and flow rate were obtained by applying the engineering hot channel factors (HCFs) for power, F_q, and flow, F_b, to the nominal operating conditions. As discussed in Section V.6, the HCFs account for fuel and assembly design tolerances and for uncertainties in various calculated and measured parameters. Combining the individual components assuming uncorrelated uncertainties, the values for F_q and F_b from Table 11 on page 24 give the following LSSS values:

   $$P_{LSSS} = P_{nom} \times F_q = 1 \text{ MW} \times 1.25 = 1.25 \text{ MW (max)}$$

   $$Q_{LSSS} = Q_{nom} / F_b = 1700 \text{ gpm} / 1.24 = 1370 \text{ gpm (min)}$$

   The value for power is unchanged from the previous TS value, but the LSSS value of flow is greater than the previous value of 1170 gpm.[34]

   Note also that the value of the pool water height was 24.25 feet in all the calculations performed here and the worst case core inlet temperature was 43.3 ^{o}C (110 ^{o}F). Thus, the previous LSSS values for water height (24.25 feet) and inlet coolant temperature (108 ^{o}F) do not need to be changed since the values used here are similar to or more conservative than

the previous values. Thus, the full set of recommended Limiting Safety System Setting (LSSS) for forced convection are

P = 1.25 MW (max) W = 1370 gpm (min)

T_{in} = 108 ^{o}F (max) L = 24.25 feet (min)

The only change from previous values is for the flow rate, W = 1370 gpm.

4. There are no changes needed for the values in Section 2.2.2 for the limiting safety settings (LSSS) for natural convection flow. This statement is also true for the Limiting Conditions for Operation (LCOs) given in Section 3.0 of the Technical Specifications.[34] However, it should be emphasized that, although no changes in the numerical values are needed, a careful review and modification for many of the justifications will be required to assure they are consistent with the overall safety analysis philosophy used here.

IX. Overall Summary and Conclusions

This report, along with several of the identified references, represents final documentation for the safety analysis for the UMass-Lowell research reactor (UMLRR). The goal here was to evaluate the consequences of several postulated events so that suitable operating limits could be set to assure safe operation of the UMLRR for steady state operations and for all protected credible off-normal events. This report gathers a lot of information concerning fuel assembly geometry (including both UMLRR and WPI fuel), typical UMLRR core configurations, expected maximum radial and axial peaking factors, cumulative blade worth profiles, pump coast down characteristics, reactor kinetics information, reactivity coefficients, etc., to support the development of a series of computer models using NATCON, PLTEMP, and PARET to do the desired analyses. In particular, NATCON and PLTEMP were used to do the steady state analyses, including the study of the flow distribution among the fuel assemblies and bypass elements (i.e. radiation baskets, control blades, etc.), and PARET was used for all the transient analyses. Conservative assumptions throughout the study, coupled with the onset of nucleate boiling (ONB) point as the safety limit, establishes a large safety factor to assure safe operation of the facility under all credible postulated events.

Based on the calculations performed here, the limiting credible accident scenario for the UMLRR is a step reactivity insertion of greater than 6.4 mk (0.64 %Δk/k). However, the operational limits, referred to as the Limiting Conditions for Operations (LCOs), specify that the maximum reactivity worth of a single experiment is 5 mk (0.50 %Δk/k), and a step insertion of this magnitude, with the reactor protection system working properly, was shown to give a large margin to the ONB safety limit. Thus, no changes are required in the LCOs to continue to assure operational safety of the facility.

However, as noted in the previous section, a new analysis philosophy and a change in the LSSS value of the flow rate to Q = 1370 gpm is recommended. The change in perception is encouraged because the reliance on the steady state ONB power to flow curve in previous studies[34] is too conservative and too restrictive. And, with this change, the old LSSS flow rate of 1170 gpm is no longer justifiable. These two changes are the only major TS modifications recommended here.

Concerning additional studies, it should be noted that all the analyses performed in this study assume a single failure criterion, which implies that beyond the single initiating failure (for

example, the loss of pump flow or the failure of an experiment that causes a rapid reactivity change), the remaining reactor systems are assumed to be functioning properly. Thus, all the transient simulations assume that either a high-power or low-flow trip is triggered by the reactor protective system, which then de-energies the electromagnets on the control blade drives, causing them to drop into the core to essentially terminate the accident sequence. Additionally, this study did not look at either a partial or full loss of coolant accident (LOCA). In both these cases (i.e. for unprotected transients or a LOCA), the coolant temperatures will likely reach and exceed the coolant saturation temperature, and different flow conditions and heat transfer relationships will be needed beyond what was used in the studies performed here -- since in this work "fuel failure" was assumed if the ONB point was hit. The ONB point, of course, is not the real point of fuel failure, but expanded analyses to address the transient behavior past the ONB point were beyond the scope of this work, since this region is beyond the specified safety limit for the UMLRR. Detailed simulation within the nucleate boiling and bulk boiling regions of operation is certainly essential for power reactors analysis but, because of the design and conservative operating limits for the UMLRR, operation in this flow region is an extremely low probability event and is not credible under the single failure criterion applied in this study. Nevertheless, the analysis of unprotected transients or a LOCA event certainly represents important and interesting areas for future study.

X. References

1. "Guidelines for Preparing and Reviewing Applications for the Licensing of Non-Power Reactors, NUREG-1537," U. S. Nuclear Regulatory Commission (NRC) (Feb. 1996).
2. "Amendment No. 14 to Facility Operating License No. R-125 for the University of Massachusetts Lowell Research Reactor," NRC Docket No. 50-223 (June 2011).
3. J. R. White and J. Marcyoniak, "Comparison of the WPI and UMLRR Fuel Assembly Models," UMass-Lowell internal project documentation (July 2011).
4. J. E. Matos and K. E. Freese, "Analyses for Conversion of the Worcester Polytechnic Institute Reactor from HEU to LEU Fuel," ANL RERTR Program (August 1987).
5. J. R. White, A. Jirapongmed, L. Bobek, and T. M. Regan, "Design and Initial Testing of an Ex-Core Fast Neutron Irradiator for the UMass-Lowell Research Reactor," 2002 ANS Radiation Protection and Shielding Topical Conference, Santa Fe, NM (April 2002).
6. J. R. White, L. Bobek, and T. M. Regan, "Initial Testing of the New Ex-Core Fast Neutron Irradiator at the UMass-Lowell Research Reactor," UMass-Lowell internal project documentation (June 2002).
7. J. R. White, "Preliminary Results and Recommendations for Replacing the Flux Trap Assembly in Location D5 in the M-2-5 UMLRR Core Configuration," UMass-Lowell internal project documentation (May 2015).
8. J. Phelps et. al., "Final Safety Analysis Report for the Lowell Technological Institute Reactor," Lowell Technological Institute Nuclear Center (Sept. 1973).
9. "Report on the HEU to LEU Conversion of the University of Massachusetts Lowell Research Reactor," submitted to the US Nuclear Regulatory Commission in fulfillment of Amendment No. 12 to License No. R-125 (April 2001).

10. J. R. White and L. Bobek, "Startup Test Results and Model Evaluation for the HEU to LEU Conversion of the UMass-Lowell Research," 24th International Meeting on Reduced Enrichment for Research and Test Reactors (RERTR 2002), San Carlos de Bariloche, Argentina (Nov. 2002).
11. http://www.ceradyne.com/products/nuclear/bortec-mmc.aspx
12. Personal communication from G. Arsenault, Ceradyne Sales Engineer to T. M. Regan, UMass-Lowell Reactor Engineer (Aug. 2014).
13. J. R. White, "Preliminary Control Blade Study Results," UMass-Lowell internal project documentation (June 2015).
14. VENTURE-PC - A Reactor Analysis Code System," distributed through the Radiation Safety Information Computational Center, CCC-654 (1997).
15. "MCNP6.1: Monte Carlo N-Particle Transport Code System," distributed through the Radiation Safety Information Computational Center, CCC-810 (Aug. 2013).
16. "SCALE: A Comprehensive Modeling and Simulation Suite for Nuclear Safety Analysis and Design," ORNL/TM-2005/39 Version 6.1, distributed through the Radiation Safety Information Computational Center, CCC-785 (July 2011).
17. J. R. White, J. Marcyoniak, and M. Pike, "Overview and Validation of the VENTURE Core Models used in Support of the WPI Fuel Transfer Project," UMass-Lowell internal project documentation (Sept. 2012).
18. J. R. White, R. Gocht, and M. Ducey "Final Report on MCNP Modeling for the UMLRR and Selected Gamma Irradiation Facilities," UMass-Lowell internal project documentation (Sept. 2011). Also see a series of internal Progress Reports that document the on-going development of the MCNP UMLRR model dated Nov. 2010, Jan. 2011, and Aug. 2011.
19. J. R. White, R. Gocht, M. Pike, and J. Marcyoniak, "Validation of the 3-D VENTURE and MCNP UMLRR Core Models used in Support of the WPI Fuel Transfer Project", Research Reactor Fuel Management Conference (RRFM2012), Prague, Czech Republic (March 2012).
20. NATCON, PLTEMP, and PARET code distribution from the RERTR Program at Argonne National Laboratory (ANL) (1988 and 1999). Also see R. S. Smith and W. L. Woodruff, "Thermal Hydraulics Analysis and Safety Margins for Natural Convection Cooled Research Reactors, " RERTR Program, Argonne National Laboratory, (1987) and K. Mishima, K. Kanda, T. Shibata, "Thermal Hydraulic Analysis for Core Conversion to the Use of Low Enriched Uranium Fuels in the KUR," Research Reactor Institute, Kyoto University, KURRI-TR-258 (1984).
21. A. L. Stevens, "Thermal Hydraulic Analysis of the University of Massachusetts Lowell Research Reactor," M.S. Thesis in Energy Engineering (Nuclear Option), UMass-Lowell, (Dec. 2002).
22. W. L. Woodruff and R. S. Smith, "A Users Guide for the ANL Version of the PARET Code, PARET/ANL (2001 Rev.)," ANL/RERTR/TM-16 (March 2001). Also see C. F. Obenchain, "PARET, A Program for the Analysis of Reactor Transients," Phillips Petroleum Company, AEC Research and Development Report (Jan. 1969). This code package is distributed through the Radiation Safety Information Computational Center, PSR-516 (Feb. 2002).

Note also that the pareth2o.exe code, as distributed, incorrectly refers to the D2O properties library -- so a temporary fix was made by renaming the H2O library (pareth2o.lib) to paretd2o.lib.

23. T. P. Michaud, "Implementation of the Inverse Kinetics Method for Reactivity Calculations at the UMLRR," M.S. Thesis in Energy Engineering (Nuclear Option), UMass-Lowell, (Dec. 2011).
24. J. R. White, “Reactivity Coefficients for Use in UMLRR Transient Analyses: Quantitative Analysis and Partial Validation via Comparison with Actual Reactor Data,” UMass-Lowell internal project documentation (August 2015).
25. J. R. White, “Updated Peaking Factors for Use in the UMLRR Safety Analysis,” UMass-Lowell internal project documentation (July 2015).
26. “FSAR Supplement for Conversion to Low Enrichment Uranium (LEU) Fuel,” Document submitted for review by the NRC for conversion of the UMass-Lowell Research Reactor (May 1993).
27. Letter from J.R. Matos, RERTR Program at ANL, to J.R. White, UMass-Lowell (Jan. 1993).
28. D. Biswas, W. P. Kovacik, and J. R. White, "Evaluation of the Delayed Neutron Importance Factor with ENDF/B-V Data," Trans. Am. Nucl. Soc., 59, 318 (June 1989).
29. M. Pike, "Expanding Local Capabilities for the Computational Analysis of the UMass-Lowell Research Reactor," M.S. Thesis in Energy Engineering (Nuclear Option), UMass-Lowell (May 2013).
30. T. M. Regan, ”Control Blade Position and Timing During UMLRR SCRAM,” UMass-Lowell Radiation Laboratory internal project documentation (Aug. 2015).
31. J. R. White, “Steady-State Thermal Hydraulic Analyses in Support of the HEU to LEU Conversion Effort,” UMass-Lowell internal project documentation (Nov. 1991).
32. A. Amarnath, "Thermal Hydraulic Analyses of the HEU and the Proposed LEU Core Configurations of the UMass-Lowell Research Reactor," M.S. Thesis in Energy Engineering (Nuclear Option), UMass-Lowell (Sept. 1993).
33. “Safety Evaluation Report related to the Evaluation of Low-Enriched Uranium Silicide-Aluminum Dispersion Fuel for Use in Non-Power Reactors, NUREG-1313,” U. S. Nuclear Regulatory Commission (NRC) (July 1988).
34. “Technical Specifications for the University of Massachusetts Lowell Reactor, Amendment 13, ” University of Massachusetts Lowell.